J. metamorphic Geol., 1998, **16,** 259–279

The Meatiq dome (Eastern Desert, Egypt) a Precambrian metamorphic core complex: petrological and geological evidence

P. NEUMAYR (email: neumayr@bkfug.kfunigraz.ac.at)[1], G. HOINKES[1], J. PUHL[1], A. MOGESSIE[1] AND A. A. KHUDEIR[2]
[1]*Institute of Mineralogy-Crystallography and Petrology, Karl-Franzens University Graz, 8010 Graz, Austria*
[2]*Institute of Geology, Assiut University, Assiut, Egypt*

ABSTRACT The Meatiq basement, which is exposed beneath late Proterozoic nappes of supracrustal rocks in the Central Eastern Desert of Egypt, was affected by three metamorphic events. The ophiolite cover nappes show only the last metamorphic overprint. The M1 metamorphic event ($T \geq 750$ °C) is restricted to migmatized amphibolite xenoliths within the Um Ba′anib orthogneiss in the structurally lowest parts of the basement. Typical upper amphibolite facies M2 mineral assemblages include Grt–Zn-rich Spl–Qtz ± Bt, Grt–Zn-rich Spl–Ms–Kfs–Bt–Sil–Qtz and locally kyanite in metasedimentary rocks. The mineral assemblages Ms–Qtz–Kfs–Sil in the matrix and Sil–Grt in garnet cores indicate that peak M2 *P–T* conditions exceeded muscovite and staurolite stabilities. Diffusional equilibration at M2 peak temperature conditions caused homogeneous chemical profiles across M2 garnets. Abundant staurolite in garnet rims and the matrix indicates a thorough equilibration during M2 at decreasing temperature conditions. M2 *P–T* conditions ranged from 610 to 690 °C at 6–8 kbar for the metamorphic peak and 530–600 °C at about 5.8 kbar for the retrograde stage. However, relic kyanite indicates pressures above 8 kbar, preceeding the temperature peak. A clockwise *P–T* path is indicated by abundant M2 sillimanite after relic kyanite and by andalusite after sillimanite. M2 fluid inclusions, trapped in quartz within garnet and in the quartz matrix show an array of isochores. Steepest isochores (water-rich H_2O-$CO_2 \pm CH_4/N_2$ inclusions) pass through peak M2 *P–T* conditions and flatter isochores (CO_2-rich H_2O-$CO_2 \pm CH_4/N_2$ inclusions) are interpreted to represent retrograde fluids which is consistent with a clockwise *P–T* path for M2. The M3 assemblage Grt–Chl in the uppermost metasedimentary sequence of the basement limits temperature to 460 to 550 °C. M3 temperature conditions within the ophiolite cover nappes are limited by the assemblage Atg–Trem–Tlc to < 540 °C and the absence of crysotile to > 350 °C. The polymetamorphic evolution in the basement contrasts with the monometamorphic ophiolite nappes. The M1 metamorphic event in the basement occurred prior to the intrusion of the Um Ba′anib granitoid at about 780 Ma. The prograde phase of the M2 metamorphic event took place during the collision of an island arc with a continent. The break-off of the subducting slab increased the temperature and resulted in the peak M2 mineral assemblages. During the rise of the basement domain retrograde M2 mineral assemblages were formed. The final M3 metamorphic event is associated with the updoming of the basement domain at about 580 Ma along low-angle normal faults.

Key words: Panafrican; Prepanafrican basement, polymetamorphism, metamorphic fluid inclusions; Proterozoic.

INTRODUCTION

The study of the characteristics and genesis of metamorphic domes, which occur in many orogenic belts worldwide, has brought important insights into the geological evolution of such terranes (e.g. Crittenden *et al*., 1980 and references therein). In the North American Cordillera, metamorphic core complexes consist typically of a high-grade metamorphic basement separated from a low metamorphic grade upper plate by a brittle detachment surface (Coney, 1980). The exhumation of metamorphic core complexes is interpreted to have occurred during extensional listric faulting, detachment of the upper section of the basement and updoming of the mantle, associated with an elevated thermal flux (Lister & Davis, 1989). However, several other mechanisms such as (1) crustal stacking and gravitational collapse (e.g. Platt, 1986), (2) delamination of supracrustal layers along a rheologically weak zone (e.g. Wijbrans *et al*., 1993), (3) removal of the lithospheric root beneath a collisional orogen (e.g. Vissers *et al*., 1995) and (4) displacement accommodation within strike-slip domes (Neubauer *et al*., 1994) have also been proposed for the exhumation and uplift of metamorphic core complexes.

Early studies compared the Meatiq dome, one of the metamorphic basement domes in the Eastern Desert of Egypt, with metamorphic core complexes in the North American Cordillera (Sturchio *et al*., 1983a). Similarities of the Meatiq basement complex with

Cordilleran metamorphic core complexes include the existence of a gneissic core, the lack of penetrative deformation in the cover rocks, unidirectional mineral and slickenside lineations and a decrease in the intensity of foliation and lineation (Sturchio *et al*., 1983a). However, Sturchio *et al*. (1983a) noted the lack of an abnormally steep metamorphic gradient between the carapace and cover. Subsequent studies described the Meatiq basement either as an old, highly metamorphosed basement, tectonically overlain by low-grade metamorphic nappes of ophiolitic and arc character that formed during at least two orogenies (e.g. Habib *et al*., 1985; El Gaby *et al*., 1990); or as a complex of the basement rocks and the covering nappes which formed during one orogeny without a significant lithological and metamorphic break between the basement and the cover sequences (e.g. Ries *et al*., 1983).

Most of the previous studies have used mainly geological, structural or isotopic evidence to decipher the evolution of the origin of the metamorphic gneiss domes in the Eastern Desert in general and the Meatiq dome in particular (Sturchio *et al*., 1983a; Stern & Hedge, 1985; El Gaby *et al*., 1990; Greiling *et al*., 1994; Kröner *et al*., 1994). Neither of these studies presented quantitative estimates of the metamorphic grade in the basement and the cover nappes. Preliminary estimates of the metamorphic grade for the Meatiq dome indicated an amphibolite facies metamorphic overprint within the dome and greenschist facies in the cover ophiolite and island arc volcanic rocks (Habib *et al*., 1985; El Gaby *et al*., 1990). In particular, a pervasive late-stage mylonitic deformation within the basement resulted in abundant retrogression of early high-grade metamorphic mineral assemblages. Therefore, high-grade mineral assemblages are only locally preserved in relict mineral textures and have not been described in earlier publications.

The purpose of investigating the Meatiq basement and the cover nappes using petrological studies was threefold: (1) To determine the P–T evolution of both units in terms of the number and grade of metamorphic events, (2) to use the metamorphic data to assist in deciphering the tectonic evolution of a structurally complex terrane, and (3) to test whether metamorphic data are consistent with a metamorphic core complex model.

GEOLOGICAL SETTING

Meatiq geology

In the Central Eastern Desert (CED) of Egypt, late Proterozoic metamorphic basement domes such as the Gebel Meatiq, Gebel El Sibai, Gebel El Shalul and Hafafit-Migif areas are exposed beneath nappes of ophiolite and island arc volcanic successions (e.g. El Gaby *et al*., 1990). The latter consist of an association of low-grade metamorphosed sedimentary and mafic volcanic rocks including gabbros and serpentinites ('ophiolitic melange': Shackleton *et al*., 1980) which are unconformably overlain by largely unmetamorphosed intermediate to silicic volcanic rocks (Dokhan volcanics) and molasse-type clastic sedimentary rocks (Hammamat; El Gaby *et al*., 1990).

The Meatiq basement dome is located ≈ 80 km west of Quseir, north of the Quseir-Qift road in the CED, and comprises a central gneiss complex (Um Ba′anib gneiss) overlain by a dominantly metasedimentary succession of quartz-rich schists which are locally intercalated with metapelitic rocks (Figs 1 & 2). The Um Ba′anib granitic to granodioritic gneiss contains lenses of aegirine-bearing alkali metagranite and locally hosts xenoliths of both partly migmatitized amphibolite, which are several hundred metres in length. A continuous layer of garnet- and biotite-bearing metapelites, which reaches up to several hundred metres in thickness along the south-western margin of the dome, occurs within the overlying metasedimentary succession. Subordinate amphibolite lenses and marbles are intercalated with these metapelites. The gneisses and metasedimentary schists are intruded by syntectonic (Abu Fannani granodiorite/tonalite, 614 ± 8 Ma; conventional zircon U–Pb age, Stern & Hedge, 1985) to posttectonic granitoids (Arieki granite, 585 ± 14 Ma, conventional zircon U–Pb age, Sturchio *et al*., 1983a), which occupy about 25% of the dome area (Fig. 1).

The contact of the basement units with the ophiolitic nappes is intensely overprinted by deformation and, along the southern margin of the Meatiq dome, intruded by the syntectonic Abu Fannani granodiorite/tonalite. Therefore, the exact location of the contact is difficult to determine. In this study, the ophiolite nappe/basement contact has been set at the lithological change from dominantly Bt–Grt–Chl schists to serpentinites and greenschists. A remnant of the ophiolite rocks occurs within the dome at the top of the basement south of the Arieki tonalite, indicating that the whole basement was originally covered by the ophiolite nappes.

Structural framework

The main features of the structural history of the Meatiq basement dome and the ophiolite nappes are summarized in Table 1 (after Habib *et al*., 1985; Fritz *et al*., 1996). There is only limited information on the style of the earliest deformation phase D1, documented by intense folding of amphibolite migmatites which occur as inclusions in the Um Ba′anib gneiss. It follows that the amphibolite migmatites have been intruded by the Um Ba′anib granitoid subsequent to D1. The D2 deformation event is preserved in relict, ductile, tight to isoclinal folds, outlined by ilmenite inclusion trails in garnet.

During D3 a penetrative mylonitic foliation developed. Displacement directions parallel to stretching are consistently top to the NW (Fritz *et al*., 1996). The S3 foliation planes are outlined by muscovite and

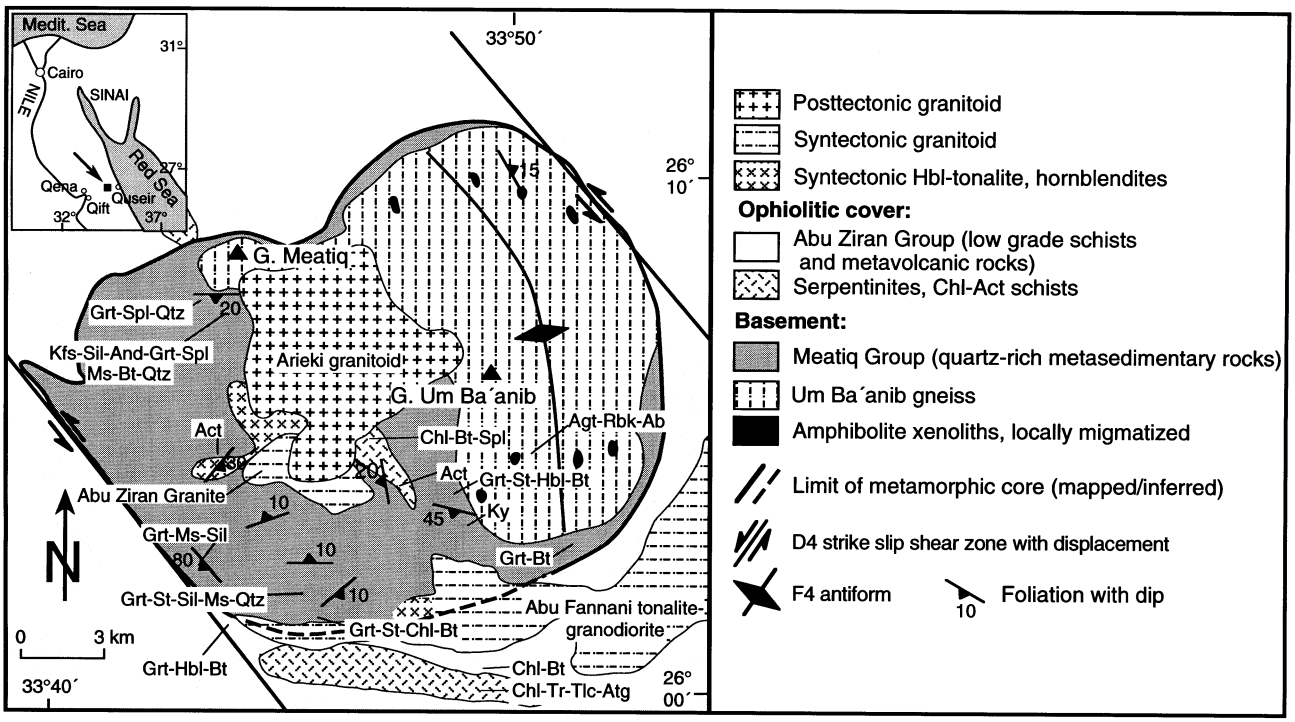

Fig. 1. Outline geological map showing important structures in the Meatiq basement complex in the Central Eastern Desert of Egypt. The distribution of critical mineral assemblages is shown for the various rock types and the limits of the basement outcrop are indicated.

Table 1. Generalized geological history of the Meatiq basement dome and its ophiolitic mélange cover sequence.

Age (Ma)	Cover sequence	Metamorphism	Age (Ma)	Basement	Metamorphism
			579 ± 6[6]	Intrusion of postkinematic granitoids (Arieki tonalite); F5 folds coeval activation of NW-striking strike-slip shear zones and S- and N-directed low-angle normal faulting during uplift of the gneiss dome	
			585 ± 14[4]		
			595.9 ± 0.5[5]		
			588.2 ± 0.3[5]		
614 to 588	normal faulting, megascale strike-slip shear zones; in the external parts of the orogen (W of the Meatiq basement) development of fold and thrust belt	(lower?) greenschist facies	613 ± 5[3]	D4 mainly extensional crenulation cleavage (ECC) in metasedimentary rocks, chlorite growth in extension fractures in garnet; F4 Um Ba′anib antiform	
			626 ± 2[3]	intrusion of syntectonic granitoids	M3 greenschist facies
			614 ± 8[4]		
			>616	D3 planar (S3) foliation in the metasedimentary rocks, non coaxial fabrics including stretching of Grt (L3), initiation of megascale strike-slip faults	
? to 614	obduction of the ophiolitic mélange onto the basement, thrusting		>626	D2 ductile open to isoclinal and tight folds outlined by internal ilmenite trails in garnet; high T gneiss fabric in the Um Ba′anib gneiss	M2 upper amphibolite facies (610–690 °C, 6–8 kbar)
			780[2]	Intrusion of the Um Ba′anib granitoid	
880–690[1]	formation of oceanic crust		>780[2]	D1 migmatization of amphibolites, which are subsequently included in the Um Ba′anib gneiss; melt enhanced extensional fabrics	M1 migmatization (750–800 °C)

Structural evolution modified after Habib *et al.* (1985), Fritz *et al.* (1996) and this study. Metamorphic evolution this study. [1] Stern (1994) and references therein; [2] U. Klötzli (pers. com., 1996), Pb single zircon evaporation age; [3] Sturchio *et al.* (1983b), Rb/Sr isochron age; [4] Stern & Hedge (1985), conventional U/Pb age on zircons; [5] Fritz *et al.* (1996), $^{40}Ar/^{39}Ar$ on muscovite; [6] reported in Sturchio *et al.* (1983a), Rb/Sr model age.

quartz in the metasedimentary schists. The D3 deformation event caused non-coaxial fabrics such as a pronounced stretching lineation, outlined by elongated garnet and tight folds in the lower sections of the metasedimentary rocks. Although Habib *et al.* (1985) distinguished up to six thrust sheets within the metasedimentary cover of the Um Ba′anib gneiss, field relations mapped during this study indicate that lithological variations in the metasedimentary complex may represent primary sedimentary features. The metasediments are therefore summarized to one single unit in Fig. 2.

During D4, S3 foliation planes are rotated into NW-striking strike-slip shear zones which developed

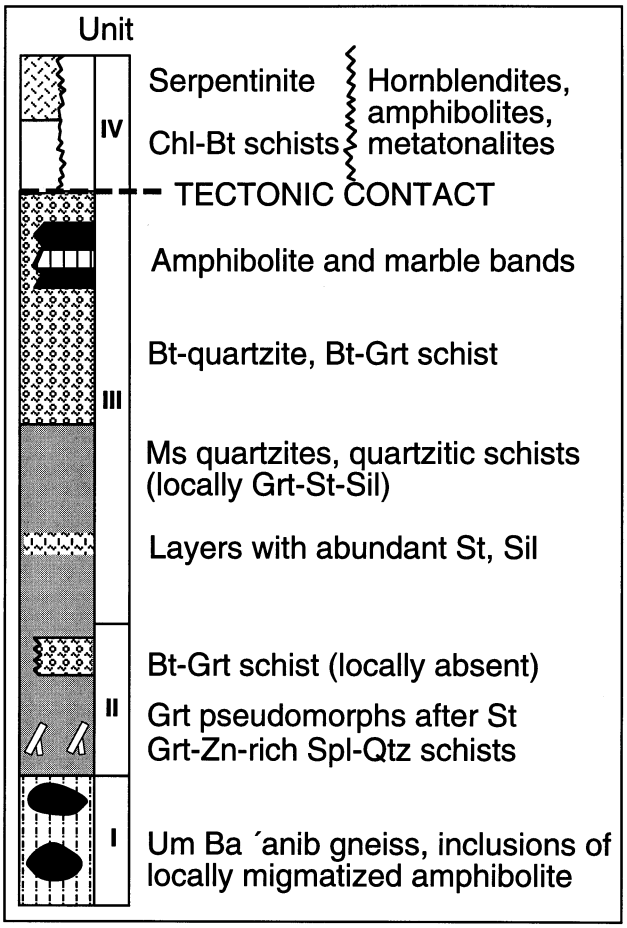

Fig. 2. Schematic profile through the Meatiq basement and the lower sections of the ophiolite and island arc cover series.

along the south-western and north-eastern margin of the Meatiq dome (Wallbrecher *et al.*, 1993; see Fig. 1). South-east of the Meatiq dome ENE-trending faults in the orientation of Riedel shear zones indicate overall sinistral slip along the main shear zone. The synkinematic Abu Fannani granodiorite/tonalite intruded along one of these ENE-trending D4 extensional faults. Fritz *et al.* (1996) determined the age of the strike-slip shear zones and the extensional faults to be 596 and 588 Ma, respectively, with $^{40}Ar/^{39}Ar$ dating of muscovite, which is within the range of the age of the synkinematic granitoids (Table 1). Updoming occurred during F4 megascale folding along NW-trending fold axes and E-W compression in the Meatiq dome (Habib *et al.*, 1985; Fritz *et al.*, 1996). E-W-trending low-angle normal faults in the metasedimentary schists caused top to the south transport at the southern margin of the dome and top to the north transport at the northern margin of the dome. F4 folds are refolded by F5 subvertical open folds (Habib *et al.*, 1985) and the postkinematic tonalites intruded into the Meatiq basement at 585 ± 14 Ma (Stern & Hedge, 1985).

PETROGRAPHY

In the Meatiq basement/ophiolite cover complex four units are distinguished based on their tectonic position (Fig. 2). The lowermost unit I comprises the Um Ba′anib gneiss and included mafic xenoliths. Unit II is the immediate metasedimentary cover comprising metaquartzites and metapelites. The latter are typically characterized by the presence of Zn-rich spinel and the lack of staurolite which contrasts with unit III. This unit includes the upper part of the metasedimentary cover and is characterized by the lack of spinel but locally abundant staurolite. Unit IV comprises ophiolite and island arc assemblages covering the basement mainly outside the domal structures. Mineral abbreviations in the text, figures, figure captions and Tables are after Kretz (1983).

Unit I: Um Ba′anib gneiss

The ovoid shaped outcrop of Um Ba′anib gneiss is the structurally lowest section of the Meatiq basement (Figs 1 & 2). The gneiss is mineralogically homogeneous and is composed of the equilibrium assemblage plagioclase, microcline, quartz and locally hornblende. In some samples of the Um Ba′anib gneiss, aegirine and riebeckite were detected as minor phases (i.e. Samples M3 and NM90 in Table 2). The gneiss is intensly foliated, probably due to D2 deformation and characteristically contains strongly folded mafic xenoliths which are up to several tens of metres in size. D1 structures of the mafic lenses are truncated at its borders by the S2 foliation of the Um Ba′anib gneiss.

The mafic lenses within the Um Ba′anib gneiss range in composition from amphibolite to hornblende gneiss. Some of these lenses are migmatized and contain bands of leucosome, which are up to 2 cm in width (Fig. 3a). The amount of leucosome in the amphibolite migmatite inclusions in the Um Ba′anib gneiss was estimated as 10–30% from the outcrop. Leucosome layers contain dominantly plagioclase and quartz, whereas the palaeosome consists of hornblende, plagioclase and quartz. Migmatized amphibolite lenses contain abundant magnetite with ilmenite lamellae.

Non-migmatized amphibolites contain the equilibrium mineral assemblage hornblende, plagioclase and quartz. Biotite typically forms rims around subhedral hornblende grains (Sample M56 in Table 2). Plagioclase is typically retrograded to fine-grained sericite. Locally, pale-green clinopyroxene occurs in bands which alternate with bands containing hornblende, plagioclase and quartz (Sample GML79 in Table 2). Fine-grained, subhedral titanite is present as an accessory phase.

Unit II: the lower metasedimentary sequence

The immediate metasedimentary cover of the Um Ba′anib gneiss is mainly quartz-rich with intercalations of metapelites (Fig. 2). Two characteristic mineral assemblages are recorded in these rocks. These are: (1) Grt–Spl–Qtz $\pm$ Bt, and (2) Grt–Spl–Ms–Kfs–Bt–Sil–Qtz.

South of the Gebel Meatiq, quartz-rich mica schists are composed of mineral assemblage (1) (Sample M35C, Table 2). Spinel occurs in the matrix in equilibrium with quartz and as inclusions within garnet and is Zn-rich. Garnet, Zn-rich spinel as well as quartz inclusions in both minerals are typically elongated, indicating contemporaneous growth of both garnet and spinel. Some garnets are composed of two cross-cutting laths with a habit similar to penetration twins of staurolite (two laths including angles of 30° to 60°, Fig. 3b) which are interpreted as pseudomorphs of garnet after staurolite.

Locally, pelitic schists contain the mineral assemblage Grt–Spl–Ms–Kfs–Bt–Sil–Qtz (Sample NM116, Table 2). Embayed grain boundaries of muscovite and quartz in contact with newly formed alkali feldspar and sillimanite document that the muscovite (Ms1) and quartz-out reaction was overstepped during prograde metamorphism (Fig. 4 a & b). Kyanite is only locally present in the rock matrices as a relict phase rimmed by another fine-grained Al_2SiO_5 polymorph, possibly sillimanite or andalusite (Sample NM38,

Table 2. Mineral assemblages from amphibolites and metasedimentary rocks from the Meatiq basement and the ophiolite and island arc volcanic rocks.

Sample	Rocktype	Remarks	Unit	Qtz	Pl	Kfs	Grt	St	Ky	Sil	And	Ms	Par	Bt	Cpx	Hbl	Spl	Ilm	Ttn	Ap	Chl	Ep/Clz	Atg
GML79	amphibolite		I	X	X										X	X			a				
M56	amphibolite		I	X	X									a		X		X	X	a	a	a	
M3	Um Ba′anib gneiss		I	X	X	X								X				a	a		a		
NM90	Um Ba′anib gneiss		I	X	X	X									X[6]	X[7]							
M223	metasediment		II	X			X					X					X,I						
M35C	metasediment		II	X			X					X		a			X						
NM116	metasediment		II	X		X	X			X	X	X		X			X						
NM38	metasediment		III	X	a				X	X[?]		X						a					
M138/1	metasediment	Hbl layer[3]	III	I,X	X		X							a		I,X		I,X			X[2]	a	
M138/1	metasediment	Hbl-free[3]	III	I,X	X		X	I,X						X				I,X			X[2]		
ED63	metasediment		III	I,X	I,X		X	I,X		I,X		I,X	X[1]	a				I,X			a		
M10	metasediment		III	X			X					X		X[2]									
ED50	metasediment		III	X	X		X					X		X,I				I,a	a				
M17	metasediment		III	X			X	I				I,X		X				I,a		a	X[2.5]		
M123	metasediment		III	X	a		X	X				a		X				X			X		
MPJ139	serpentinite		IV														a[g]						X
MPJ143	ultramafic schist		IV													X[9]	a[g]				X		X
M13	epidote amphibolite		IV													X		X		X		X	

I = inclusion in Grt, X = major phase, a = accessory phase, [1] = rim around Ms, [2] = in pressure shadow or fractures of Grt, [3] = layering on thin-section scale, [4] = inclusions in Ms, [5] = overprinting main foliation, [6] = aegirine, [7] riebeckite, [8] = chromite, [9] = tremolite.

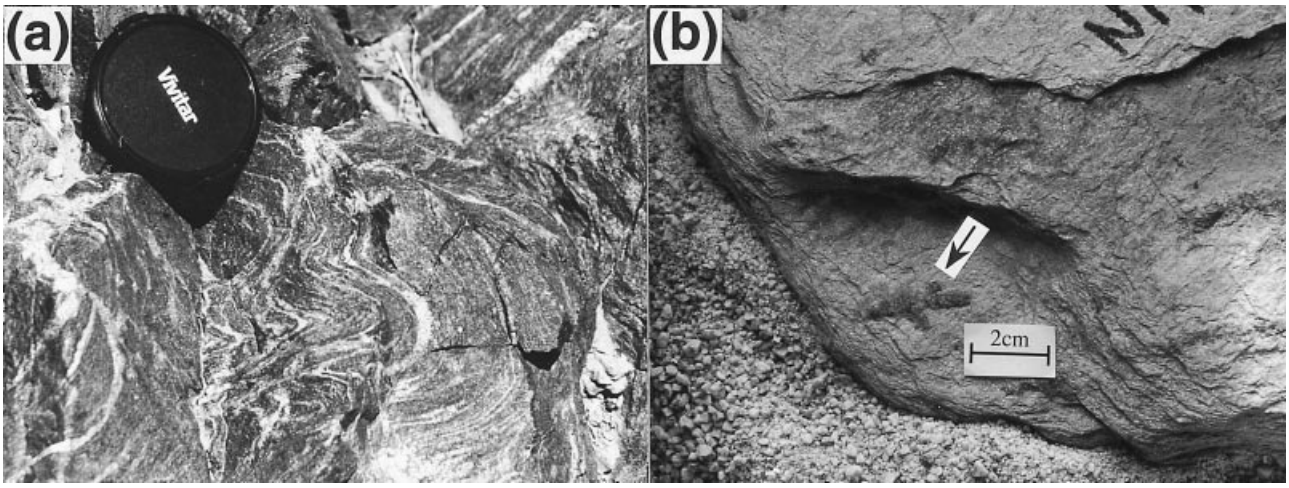

Fig. 3. Photographs of representative outcrops and hand specimen of (a) a migmatitized amphibolite xenolith in the Um Ba′anib gneiss, and (b) an arrangement of garnet laths, interpreted to represent pseudomorphs after staurolite interpenetration twins in unit II.

Table 2, Fig. 4c). Fibrolitic sillimanite is the dominant Al_2SiO_5 polymorph of the matrix. Its occurrence as clusters may indicate that sillimanite has replaced kyanite. The sillimanite clusters in sample NM116 are typically rimmed by andalusite (Fig. 4d). Needle shaped aggregates, up to several millimetres in length, are composed of fine andalusite grains. Both textures are interpreted to represent retrograde replacement of sillimanite and/or kyanite by andalusite.

The dominant foliation as outlined by muscovite (Ms2) and fine-grained recrystallized quartz and plagioclase is related to D3. D4 caused a brittle deformation of garnet (Fig. 5b) and a mylonitic foliation, outlined by fine-grained sericite (Ms3) which overprints medium-grained subhedral muscovite (Ms2; Fig. 5a).

Unit III: the upper metasedimentary sequence

The upper metasedimentary cover contains two different garnet generations. Type Grt1 occurs either elongated, parallel to S2 foliation, or as porphyroblasts with diameters of up to 1 cm (Fig. 6). Individual porphyroblastic grains of Grt1 may be either rimmed by, or completely recrystallized to, a chemically different generation of euhedral Grt2. Porphyroblastic as well as deformed Grt1 locally hosts inclusions of tight to isoclinally folded (F2) ilmenite trails (Sample M138/1, Table 2; Fig. 5c). These folded trails within Grt1 as well as recrystallized and deformed plagioclase in the matrix indicate that these mineral assemblages have formed and have been deformed subsequently to at least amphibolite facies conditions during D2 and D3 deformations. Staurolite inclusions occur preferentially in Grt2 (Sample M138/1, Table 2, Fig. 6). The matrix in these schists is composed of bands of Pl–St–Bt–Ilm alternating with bands of Pl–Hbl–Qtz–Ilm. Hornblende only occurs in bands that do not contain staurolite.

Locally, porphyroblastic Grt1 contains abundant fibrolite inclusions only in the core and staurolite inclusions only at the outermost rims and at the contact to Grt2 (not containing other inclusions except staurolite; sample ED63, Table 2, Fig. 5d). Minor

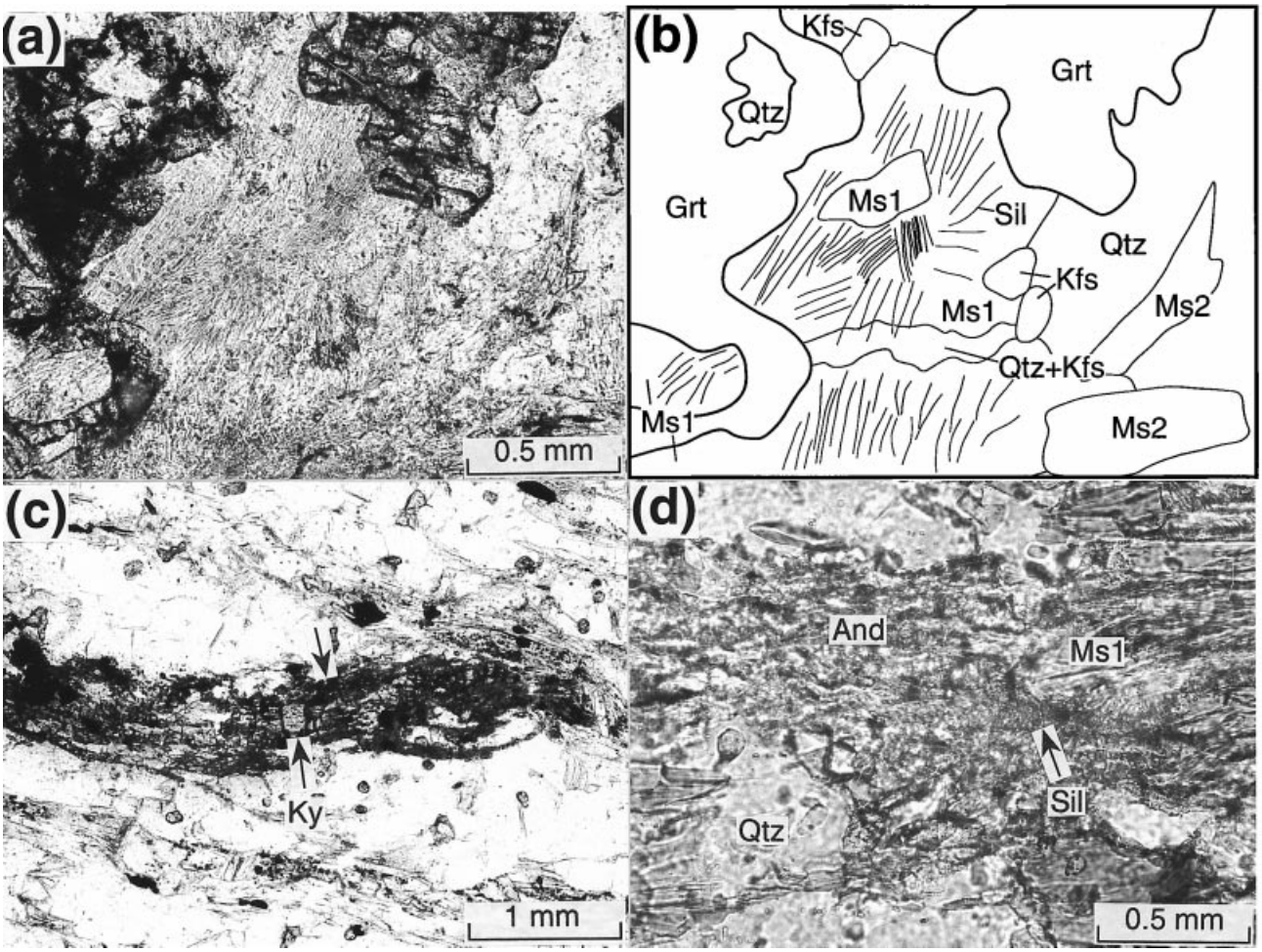

Fig. 4. Photomicrographs of typical Al_2SiO_5 mineral textures in unit II. (a) Reaction texture of Ms1 and quartz forming alkali feldspar and sillimanite (sample NM116); (b) sketch of photomicrograph in Fig. 4 A at the same scale; (c) kyanite is replaced by a second, unidentified Al_2SiO_5 polymorph (sillimanite or andalusite: arrowed; sample NM38); (d) sillimanite is replaced by andalusite (sample NM116). (All photographs are taken in transmitted plane-polarized light).

plagioclase and Ms1 occur as inclusions in Grt1 of the same sample. The matrix in these schists is composed of the equilibrium assemblage St–Sil–Ms–Qtz. Matrix muscovite may be replaced by a paragonite–margarite intergrowth at its rims.

In areas that are strongly deformed by D3 and D4 deformations, Grt 1 and 2 are elongated parallel to the S3 foliation. Towards the southern margin of the basement and closer to the basement/cover nappe boundary, metapelitic schists are characterized by a chlorite-rich matrix which shows equilibrium textures with garnet. Biotite and staurolite in these rocks typically exhibit irregular grain boundaries which indicates that both minerals are unstable with respect to chlorite and garnet (Grt3, sample M123, Table 2). Fractures in Grt 1 and 2 in the whole metasedimentary sequence of the basement are typically filled with chlorite. This chlorite growth in the fractures is interpreted to be contemporaneous with the abundant chlorite growth in the matrix close to the basement/cover nappe boundary.

Unit IV: metamorphosed basic and ultrabasic rocks of the ophiolite and island arc nappes

In the ophiolite and island arc cover nappes surrounding the Meatiq basement, the main rock types are serpentinites, talc-tremolite schists, greenschists and epidote amphibolites which are all characterized by upper greenschist- to lower amphibolite facies mineral assemblages. The serpentinites contain dominantly fine-grained needles of antigorite (up to 95 vol% of the rock), minor relictic chromite and late-stage carbonate alteration. Locally, metaperidotites contain magmatic relicts of olivine and clinopyroxene which are replaced by antigorite and tremolite and which is also the equilibrated mineral assemblage in the rock matrix. The serpentinites are transected by discrete shear bands (low-angle normal faults) which are composed of tremolite, talc and chlorite. The equilibrium assemblage indicates that normal faulting occurred under greenschist facies metamorphic conditions. The most abundant rock type within these ophiolite nappes is epidote amphibolite. These consist of amphibole, epidote/zoisite and locally minor chlorite and calcite. Ilmenite and magnetite are the opaque accessory phases. Plagioclase occurs only in gabbroic-textured rocks. The local occurrence of diopside and grossular-rich garnet indicates more Ca-rich whole-rock chemical compositions due to metasomatic reactions (metarodingite).

Ophiolite nappes within the Meatiq core lying on top of the basement are indistinguishable in both rock-types and mineral compositions from the external nappes. This indicates similar metamorphic conditions for both nappes. Tonalites, hornblendites and gabbros of the internal nappes show magmatic amphiboles which are overgrown by thin actinolite rims. These rims are consistent with a greenschist facies metamorphic grade.

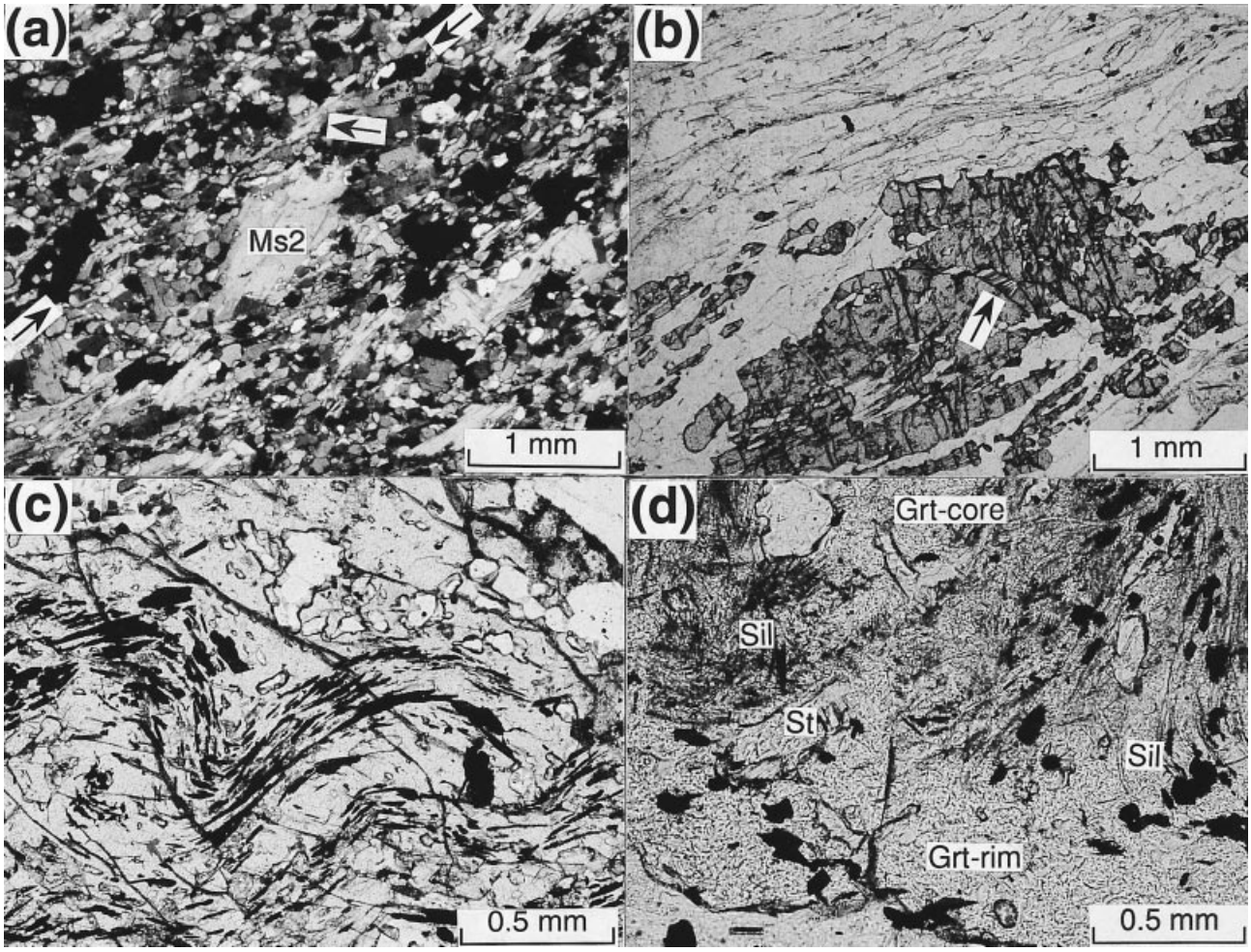

Fig. 5. Photomicrographs of mineral textures in the metasedimentary rocks of the Meatiq basement. (a) medium-grained muscovite (interpreted to be associated with the D3 deformation) deformed by S4 foliation (indicated by the two arrows at the edge of the photomicrograph) which is outlined by fine-grained, recrystallized muscovite (indicated by arrow), plagioclase and quartz (sample M116); (b) garnet fractured during D4 deformation (fractures are filled with chlorite, see arrow), S4 foliation is outlined by fine-grained muscovite (sample M35C); (c) complexly folded (F2 folds) ilmenite inclusions trails (arrowed) in Grt1 (sample M138/1); (d) sillimanite-garnet assemblage in the core and retrograde staurolite-garnet assemblage in the rim of the garnet (sample ED63). [(a): transmitted, cross-polarized light; (b) (c) (d): transmitted plane-polarized light].

Contact metamorphic aureole adajcent to the Abu Fannani granodiorite/tonalite

Adjacent to the Abu Fannani granodiorite/tonalite, a contact metamorphic aureole within metabasites of the cover nappes was formed. Hornfels bands with granular textures reach up to metres in width and contain porphyroblastic garnet, hornblende and biotite. Locally, the hornfelses consist of 90 vol% euhedral garnet which are characterized by radial trails of ilmenite and other not identified, very fine-grained opaque minerals. This texture probably indicates fast garnet growth during contact metamorphism.

MINERAL CHEMISTRY OF METAMORPHIC PHASES

Chemical analyses have been obtained using a ARL-SEMQ electron microprobe, with 15 kV accelerating voltage and 20nA sample current on brass. The analyses were calibrated using internationally recognized mineral standards and standard ZAF correction methods. Representative mineral analyses are given in Tables 3, 4 & 5; a fuller dataset is available via the JMG Homepage at one of the Web sites. Element distribution images were produced using a JEOL-JSM6310 scanning electron microscope at an accelerating voltage set to 15 kV. Both instruments are at the Institute of Mineralogy-Crystallography and Petrology, Karl-Franzens University Graz.

Garnet in most metapelitic schists is almandine rich ($X_{Alm} = 0.58–0.81$, depending on the whole-rock chemical composition) with minor pyrope, grossular and spessartine components (Tables 4 & 5). Garnet in quartz-rich schists contains a higher almandine component ($X_{Alm} = 0.91$) than those from pelitic schists. Deformed garnet 1 porphyroblasts from units II and III show small chemical variations from core to rim

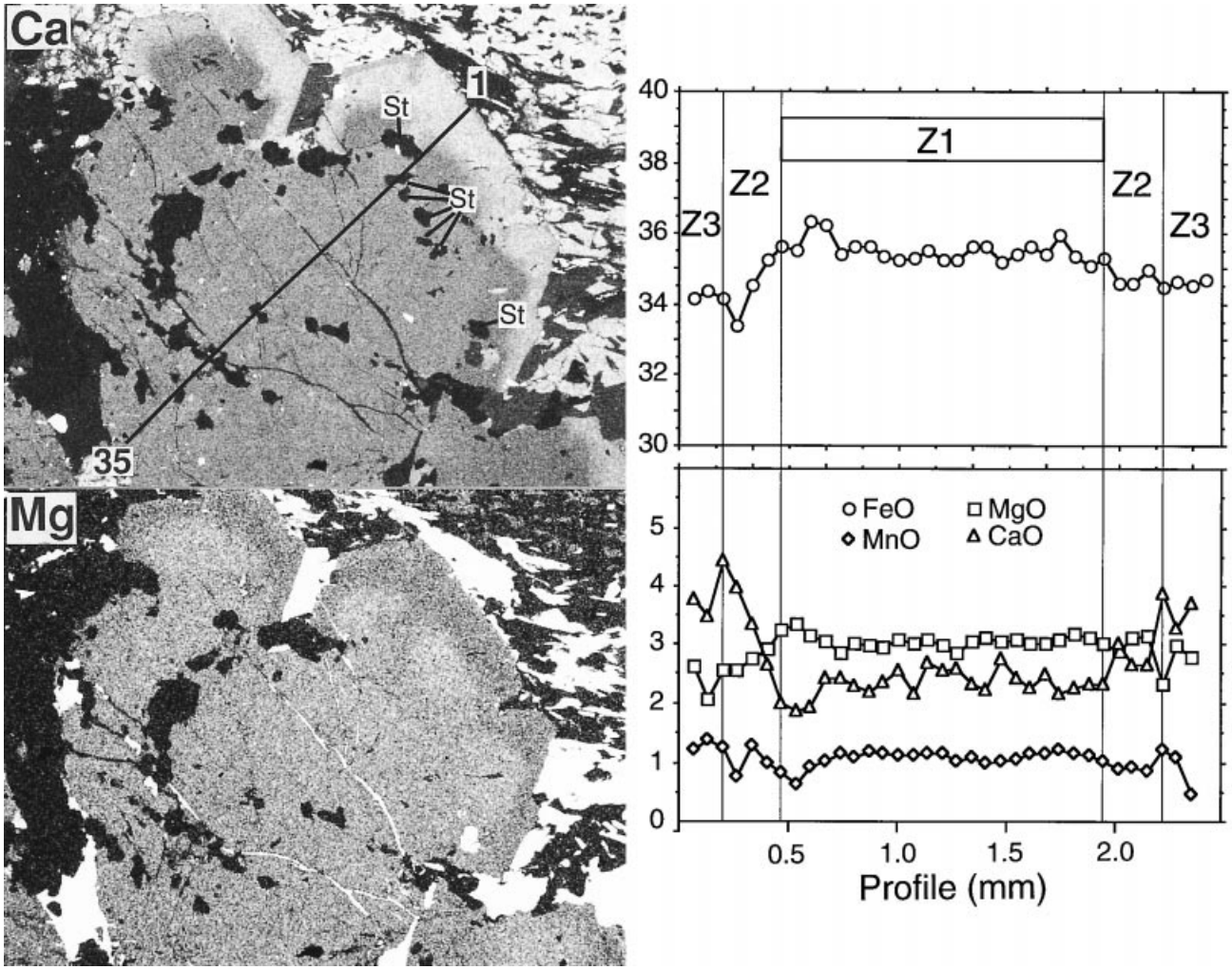

Fig. 6. Backscattered distribution images for Ca and Mg and line-scan for FeO, MnO, MgO and CaO (in wt%) across a Grt1 core which is rimmed by euhedral Grt2 (sample M138/1, unit III of the basement). The position of the scan is indicated by labelled line in the Ca distribution image (1 marks the begin and 35 the end of the line scan). Note the homogeneous elemental abundance in the core of the garnet. The location of staurolite inclusions are labelled. All other inclusions in the garnet are quartz. Z1 to Z3 marks zones of similar chemical variation and are based on the chemical profile.

(Figs 6 & 7). Compositional variation within the core of the garnet (Grt1) are either negligible (zone Z1 in Fig. 6) or characterized by some enrichment of Mn and Fe (zone A1 in Fig. 7) and, in some cases, Ca in the core (zone A1 in Fig. 7). Garnet rims (Grt2) show a typical increase in Ca (e.g. X_{Grs} from 0.07 in the core to 0.13 in the rim) and Mn and a decrease in Mg and Fe (zones Z2, A2, B2 in Figs 6 & 7). The profile across a garnet with sillimanite inclusions in the core and staurolite inclusions in the rim shows a minor increase in Ca and a decrease in Fe and Mg towards the rim (Fig. 7b). The Fe/(Fe + Mg) ratio of the garnet increases slightly from the core (0.92) to the rim (0.95).

Spinel is gahnite–hercynite with X_{Gah} between 0.69 and 0.80 and the Fe/(Fe + Mg + Zn) ratio between 0.19 and 0.30 (sample M223; Table 4). Spinel inclusions in garnet are chemically similar to spinel coexisting with quartz in the matrix ($X_{Gah} = 0.71$–0.81). Medium-grained spinel is typically zoned from $X_{Gah} = 0.69$ at the rim to $X_{Gah} = 0.80$ in the core. However, spinel inclusions in muscovite are characterized by a lower X_{Gah} of 0.68 which is similar to the rim compositions of medium-grained spinel. The Cr_2O_3 content in all spinels is < 1 wt%.

Staurolite is Fe-rich ($X_{Fe} = 0.82$) and contains variable amounts of ZnO (0.05 wt% to 1.68 wt% ZnO, Tables 4 & 5) with irregular variation of the ZnO content from sample to sample. Staurolite inclusions in garnet have essentially the same chemical composition as matrix staurolite (Table 5) or may be marginally higher in Fe ($X_{Fe} = 0.92$ in the inclusion and $X_{Fe} = 0.88$ in the matrix in sample ED63). Medium-grained, euhedral staurolites are essentially unzoned.

Hornblende is classified mainly as tschermakite, hastingsite and magnesio hornblende (classification after

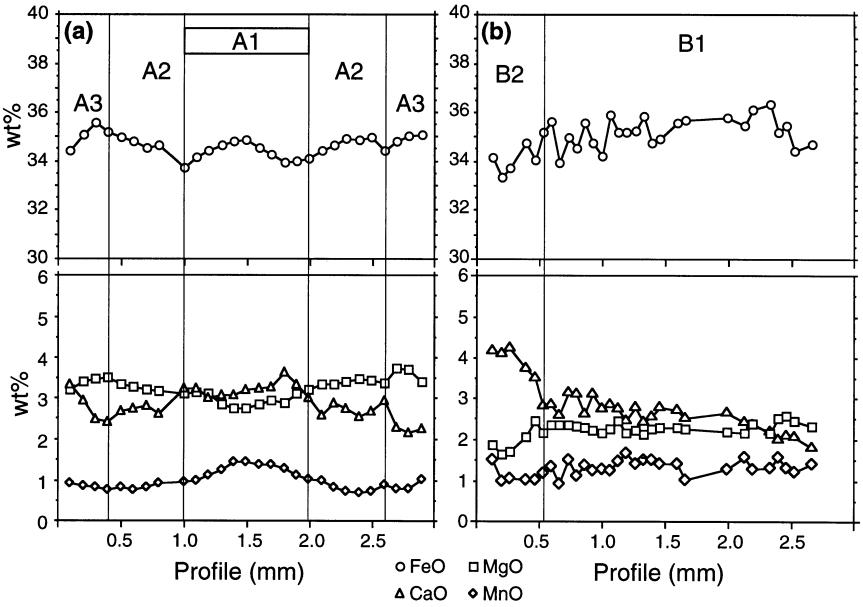

Fig. 7. Garnet zoning profiles across deformed garnets of units II and III of the basement. A1 to A3 and B1 and B2 mark zones of similar chemical variation and are based on the chemical profile. (a) Sample M138/1. Bell-shaped MnO zoning in A1. (b) Profile across half of a garnet in sample ED63 from the rim to the core. The second half of the profile has not been analysed because most of the garnet is corroded. Zone B2 indicates the garnet rim which contains staurolite inclusions (but no sillimanite) and zone B1 is the garnet core which contains abundant sillimanite inclusions.

Table 3. Representative mineral analyses of the Meatiq basement rocks.

	GML79			M56		
	I	I	I	I Pl 565	I Pl 5611	I
Zone	Pl 34	Hbl 69	Px 1	core	rim	Hbl 563
SiO_2	57.94	44.38	53.53	63.80	58.85	39.59
TiO_2	0.01	0.82	0.04	—	—	0.79
Al_2O_3	26.11	11.20	0.31	23.10	25.80	12.73
FeO	0.14		9.59	0.09	0.06	22.57
MnO	—	0.23	0.41	—	—	0.48
MgO	—	11.10	11.78	—	—	6.55
CaO	8.16	11.97	23.62	4.37	6.95	10.51
Na_2O	6.79	1.45	0.29	7.60	6.80	1.58
K_2O	0.16	0.69	—	0.24	0.15	1.26
Total	99.31	97.83	99.57	99.20	98.61	96.06
Si	2.61	6.56	2.02	2.83	2.65	6.10
Ti	—	0.09	0.001	—	—	0.09
Al	1.39	1.95	0.01	1.21	1.37	2.32
Fe^{2+}	0.01	1.51	0.30	0.003	0.002	2.91
Fe^{3+}	—	0.42	—	—	—	—
Mn	—	0.03	0.01	—	—	0.07
Mg	—	2.45	0.66	—	—	1.51
Ca	0.39	1.89	0.96	0.21	0.34	1.73
Na	0.59	0.42	0.02	0.65	0.60	0.47
K	0.01	0.13	—	0.02	0.01	0.25
Total	5.00	15.45	3.98	4.92	4.97	15.45
X_{An}	0.40	—	—	0.24	0.36	—
X_{Fe}	—	0.38	0.31	—	—	0.66

Mineral abbreviations after Kretz (1983); Oxygen basis for recalculation of the analyses: Pl, 8; Hbl, 23; Px, 6; $X_{An} = Ca/(Ca+Na)$; $X_{Fe} = Fe/(Fe+Mg)$.

Leake, 1978) in amphibolite inclusions in the Um Ba′anib gneiss with X_{Fe} of 0.38 (Table 3). Amphibole in the metasedimentary rocks of unit III is tschermakite and hastingsite (Table 4). Metamorphic amphibole in the hornblendite–tonalite cover nappes is actinolite with X_{Fe} of 0.17 and is clearly distinct from basement amphibole (Table A3, Sample NM65).

Plagioclase is zoned in migmatitized amphibolite lenses in the Um Ba′anib gneiss from $X_{An} = 0.24$ in the core to $X_{An} = 0.36$ in the rim of the grain (Table 3). Plagioclase in other amphibolite lenses within the gneiss is only poorly zoned, but varies in composition from $X_{An} = 0.20$ to $X_{An} = 0.40$ in different lenses. Plagioclase from pelitic schists contains typically a high anorthite component with X_{An} between 0.34 and 0.51. Plagioclase inclusions in garnet are similar in composition to plagioclase from the surrounding matrix.

Alkali feldspar is mostly pure K-feldspar with an X_{Ab} of 0.09.

Clinopyroxene in the amphibolite xenoliths in the Um Ba′anib gneiss that coexists with hornblende is mainly diopside with $Wo_{49}En_{34}Fs_{17}$ on average (IMA classification, Morimoto, 1988). Clinopyroxene occurs enriched in bands within these rocks. Within distinct layers, a difference in chemical composition of clinopyoxene from the centre to the rims is observed. Clinopyroxene at the centre of these bands is characterized by $X_{Fe} = 0.45$, whereas clinopyroxene at the edge of the band is more diopsidic in composition with $X_{Fe} = 0.37$, which indicates probably a whole-rock chemical control on the occurrence of pyroxene within these rocks. Clinopyroxene in the Um Ba′anib gneiss is aegirine with $Aeg_{95.50}Jad_{4.50}$.

Biotite inclusions in garnet are similar in composition to matrix biotite, but contain marginally higher Fe ($X_{Fe} = 0.78$ in the matrix and $X_{Fe} = 0.81$–0.85 in inclusions, e.g. sample ED50, Table 5).

Muscovite hosts locally between 0.05 and 0.20 paragonite component. Subhedral muscovite in sample ED 63 is overgrown by fine-grained mica which contains between 0.32 and 0.53 margarite component and between 0.42 and 0.62 paragonite component.

Table 4. Representative mineral analyses of the Meatiq basement rocks.

	M138/1										M223		M35C	
Zone	II Grt 410 core	II Grt 421 rim	II Grt 214 rim	II Bt 32 matrix	II Grt 220 rim	II St 42 inclusion	II St1383 matrix	II Pl1384 matrix	II Hbl 1381 matrix	II Chl 33 matrix	II Spl 40 rim	II Spl 43 core	II Spl 10 core	II Grt 74A rim
SiO_2	37.84	37.87	37.71	36.12	37.60	27.95	27.53	55.80	39.65	25.95	0.11	0.06	0.40	36.66
TiO_2	0.07	0.03	0.09	1.24	0.08	0.36	0.51	0.02	0.34	0.03	—	—	—	0.01
Al_2O_3	21.13	21.36	20.72	17.56	20.85	52.44	53.96	27.03	18.27	26.73	56.56	55.43	55.78	20.52
FeO	35.11	32.92	34.86	20.53	34.55	12.89	11.61	0.19	19.77	7.21	12.27	8.66	11.71	40.06
MnO	1.04	0.98	1.23	0.05	1.21	0.04	0.09	—	0.10	0.04	—	—	—	0.97
MgO	2.99	2.76	2.54	10.39	2.85	1.69	1.36	—	5.91	26.05	0.08	0.04	0.12	0.20
CaO	2.39	4.67	3.53	0.10	2.74	—	0.07	10.34	11.64	—	—	—	—	2.13
Na_2O	—	—	—	0.19	—	0.20	0.06	5.42	1.59	—	—	—	—	—
K_2O	—	—	—	9.40	—	—	—	0.05	0.56	—	—	—	—	—
ZnO	—	—	—	—	0.05	1.45	1.68	—	—	—	31.29	35.90	33.10	—
Total	100.57	100.59	100.68	95.58	99.93	97.02	96.87	98.85	97.83	86.01	100.31	100.09	101.11	100.55
Si	6.03	6.02	6.04	5.51	6.04	7.78	7.70	2.54	5.94	5.04	0.03	0.02	0.09	6.00
Ti	0.008	0.004	0.01	0.14	0.01	0.08	0.11	0.001	0.04	0.004	—		—	0.001
Al	3.97	4.00	3.91	3.16	3.95	17.36	17.79	1.45	3.22	6.12	15.56	15.81	15.71	3.96
Fe^{2+}	4.68	4.37	4.67	2.62	4.64	3.03	2.72	0.01	2.48	1.17	2.46	1.58	2.34	5.48
											—	0.17	—	—
Mn	0.14	0.13	0.16	0.01	0.17	0.01	0.02	—	0.01	0.006	—	—	—	0.13
Mg	0.71	0.65	0.61	2.36	0.68	0.71	0.57	—	1.32	7.55	0.03	0.02	0.04	0.05
Ca	0.41	0.79	0.60	0.02	0.47	—	0.02	0.50	1.87	—	—	—	—	0.37
Na	—	—	—	0.06	—	0.11	0.03	0.48	0.46	—	—	—	—	—
K	—	—	—	1.83	—	—	—	0.003	0.11	—	—	—	—	—
Zn	—	—	—	—	0.01	0.30	0.35	—	—	—	5.53	6.41	5.85	—
Total	15.95	15.96	16.00	15.71	15.97	29.38	28.72	4.98	15.45	19.89	24.01	24.01	24.03	15.99
XGah	—	—	—	—	—	—	—	—	—	—	0.69	0.80	0.71	—
XAlm	0.79	0.74	0.77	—	0.78	—	—	—	—	—	—	—	—	0.91
XSps	0.02	0.02	0.03	—	0.03	—	—	—	—	—	—	—	—	0.02
XPrp	0.12	0.11	0.10	—	0.11	—	—	—	—	—	—	—	—	0.01
XGrs	0.07	0.13	0.10	—	0.08	—	—	—	—	—	—	—	—	0.06
XAn	—	—	—	—	—	—	—	0.51	—	—	—	—	—	—
XFe	0.86	0.87	0.88	0.56	0.87	0.81	0.82	—	0.65	0.13	—	—	—	0.99

Mineral abbreviations after Kretz (1983); in addition: Gah = gahnite. Oxygen basis for recalculation of the analyses: Spl, 32; Grt, 24; St: 32; Pl, 8; Hbl, 23; Chl, 28; Bt, 22. XGah = Zn/(Zn + Fe + Mg); XAlm = Fe/(Fe + Mg + Mn + Ca); XSps = Mn/(Fe + Mg + Mn + Ca); XPrp = Mg/(Fe + Mg + Mn + Ca); XGrs = Ca/(Fe + Mg + Mn + Ca); XAn = Ca/(Ca + Na); XFe = Fe/(Fe + Mg). Grt 410 and Grt 421 represent core and rim analyses in the same garnet grain. Grt 214, Bt 32 and Grt 220, St 42 represent mineral pairs used for temperature calculations and Grt 421, St 1383, Hbl 1381 are used for pressure calculations (see Tables 5 & 6, respectively).

Chlorite occurs retrograde after garnet and biotite and is characterized by a X_{Fe} of 0.13.

Ilmenite is present as inclusions in garnet and mostly pure with MnO contents <2 wt%.

METAMORPHIC EVOLUTION

From textural observations three metamorphic events (M1, M2, M3) are recognized in the Meatiq basement, whereas only assemblages of the M3 event are present in the ophiolite and island arc cover nappes. Because the age of the M2 event has yet to be determined using isotopic systems, the distinction between the metamorphic events is based largely on petrographical and structural evidence. The petrographic description with respect to the different metamorphic events is summarized in Fig. 8 and Table 2.

The earliest metamorphic event in the Meatiq metamorphic core complex is evident in migmatized amphibolite xenoliths in the Um Ba′anib gneiss. These xenoliths contain early F1 folds (Fig. 3a) which are truncated at the amphibolite-gneiss boundary by the S2 foliation in the Um Ba′anib gneiss. In contrast to the amphibolites, migmatitic fabrics are not present in the Um Ba′anib gneiss. Therefore, the migmatization of the amphibolites, which needs significantly higher temperatures than migmatization of metagranitoids and metapelites is interpreted to be the result of a first M1 metamorphic event which occurred prior to the intrusion of the Um Ba′anib granitoid and is thus limited to the migmatized amphibolites. Because S2 fabrics clearly truncate earlier fabrics within the amphibolites and neither the Um Ba′anib gneiss nor the metasedimentary cover of zones II and III (Fig. 2) are migmatized, mineral assemblages within Um Ba′anib gneiss and the metasedimentary rocks are ascribed to a second M2 metamorphic event. Petrographically, only the leucosome caused by migmatization of the amphibolites and the zoning within the plagioclase may be ascribed to the M1 episode. All other mineral assemblages adjusted to the subsequent metamorphic events (Fig. 8).

The main equilibration of all rock units in the Meatiq basement occurred during the M2 metamorphic event. All minerals grown during the M2 event are either aligned parallel to the high-temperature S2 foliation or have been deformed during the D3 and D4 events. The garnet generations Grt1 and Grt2

Table 5. Representative mineral analyses of the Meatiq basement rocks.

	NM116		ED63							ED50						M10	
Zone	II Kfs 1161 matrix	II Ms 1162 matrix	III Grt 38 core	III Pl 3 inclusion	III Ms12 inclusion	III Ilm5 inclusion	III Pg 632 matrix	III St14 inclusion	III St10 matrix	III Grt 20 core	III Bt 2 inclusion	III Grt 50/6 rim	III Bt 50/6 matrix	III Grt24A rim	III Bt8 matrix	III Grt 335 rim	III Bt 43 matrix
SiO_2	64.64	45.89	37.00	61.26	47.65	—	41.00	28.58	28.39	37.66	34.38	37.76	34.07	37.24	34.90	36.93	40.27
TiO_2	—	0.11	0.16	0.01	0.28	50.68	0.08	0.48	0.27	0.10	2.46	0.21	3.52	0.03	3.45	0.06	0.44
Al_2O_3	19.02	35.32	20.50	24.08	35.56	—	43.52	54.20	53.97	20.85	16.04	21.03	14.90	20.87	16.73	20.91	27.25
FeO	0.08	2.97	35.82	0.27	1.27	46.19	0.46	14.18	14.68	27.46	28.84	25.99	26.90	31.45	26.55	34.84	15.38
MnO	—	0.01	3.74	0.01	—	1.15	—	0.14	0.11	3.63	0.54	5.45	0.39	4.13	0.08	4.28	0.11
MgO	—	0.12	1.15	—	0.28	—	—	0.61	1.07	0.46	2.84	0.48	4.11	0.54	4.34	0.08	0.69
CaO	—	—	1.76	6.82	0.03	—	4.33	—	—	9.76	0.09	9.91	0.12	5.63	—	2.97	0.03
Na_2O	0.97	0.35	—	8.23	1.30	—	4.57	—	—	—	0.04	—	0.18	—	0.15	—	0.32
K_2O	15.66	10.78	—	0.04	8.37	—	0.62	—	—	—	9.40	—	8.93	—	9.95	—	9.69
ZnO	—	—	—	—	—	—	—	0.20	0.05	—	—	—	—	—	—	—	—
Total	100.37	95.55	100.13	100.72	94.74	98.02	94.58	98.39	98.54	99.92	94.63	100.83	93.12	99.89	96.15	100.07	94.18
Si	2.97	6.14	6.03	2.71	6.29	—	5.34	7.89	7.84	6.04	5.57	6.01	5.56	6.04	5.49	6.03	5.91
Ti	—	0.01	0.02	—	0.03	0.99	0.01	0.10	0.06	0.01	0.30	0.03	0.43	0.01	0.41	0.01	0.05
Al	1.03	5.57	3.94	1.26	5.53	—	6.68	17.62	17.56	3.94	3.06	3.95	2.87	3.98	3.10	4.02	4.71
Fe^{2+}	0.003	0.33	4.88	0.01	0.14	1	0.05	3.27	3.39	3.68	3.91	3.46	3.67	4.26	3.49	4.75	1.89
Fe^{3+}	—	—	—	—	—	—	—	—	—	—	—	—	—	—	—	—	—
Mn	—	0.001	0.52	—	—	0.03	—	0.03	0.03	0.49	0.07	0.74	0.05	0.57	0.01	0.59	0.01
Mg	—	0.02	0.28	—	0.05	—	—	0.25	0.44	0.11	0.69	0.11	1.00	0.13	1.02	0.02	0.15
Ca	—	—	0.31	0.32	0.01	—	0.60	—	—	1.68	0.02	1.69	0.02	0.98	—	0.52	0.01
Na	0.08	0.09	—	0.71	0.33	—	1.15	—	—	—	—	—	0.06	—	0.04	—	0.09
K	0.92	1.84	—	—	1.41	—	0.10	—	—	—	1.94	—	1.86	—	1.99	—	1.81
Zn	—	—	—	—	—	—	—	0.04	0.01	—	—	—	—	—	—	—	—
Total	5.00	14.00	15.98	5.01	13.79	2.02	13.93	29.20	29.33	15.95	15.56	15.99	15.52	15.97	15.55	15.94	14.54
X_{Fe}	—	—	0.99	—	—	—	—	0.92	0.88	0.97	0.85	0.97	0.79	0.97	0.77	0.99	0.93
X_{Alm}	—	—	0.81	—	—	—	—	—	—	0.62	—	0.58	—	0.71	—	0.81	—
X_{Sps}	—	—	0.09	—	—	—	—	—	—	0.08	—	0.12	—	0.09	—	0.10	—
X_{Prp}	—	—	0.05	—	—	—	—	—	—	0.02	—	0.02	—	0.02	—	—	—
X_{Grs}	—	—	0.05	—	—	—	—	—	—	0.28	—	0.28	—	0.16	—	0.09	—

Mineral abbreviations after Kretz (1983). Oxygen basis for recalculation of the analyses: Kfs, 8; Grt, 24; St, 32; Ms, Bt, Pg, 22; $X_{Fe} = Fe/(Fe+Mg)$; $X_{Alm} = Fe/(Fe+Mg+Mn+Ca)$; $X_{Sps} = Mn/(Fe+Mg+Mn+Ca)$; $X_{Prp} = Mg/(Fe+Mg+Mn+Ca)$; $X_{Grs} = Ca/(Fe+Mg+Mn+Ca)$. Grt 38, Pl 3, Ms 12, Ilm 5 are used for pressure calculations (see Table 6).

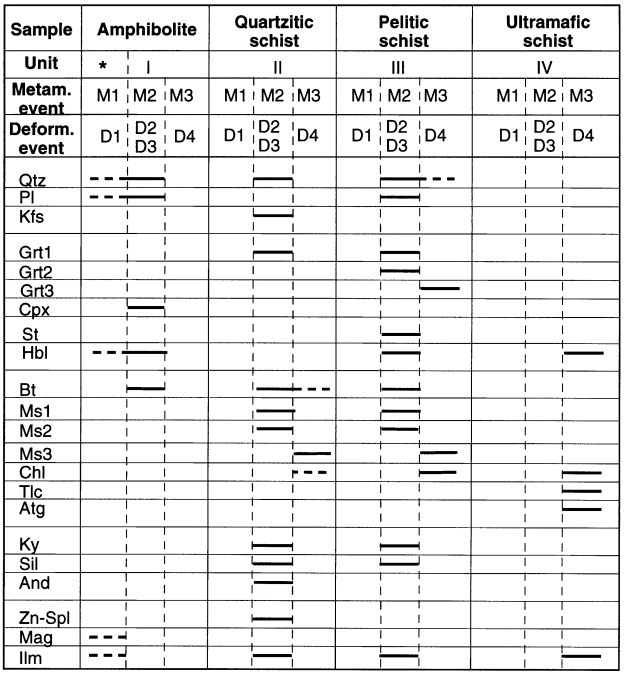

Fig. 8. Paragenetic sequence of metamorphic mineral assemblages in amphibolites, quartzitic and pelitic schists of the Meatiq basement and ultramafic schists of the ophiolite cover nappes. *M1 metamorphism refers only to the migmatized sections of the amphibolite xenoliths in the Um Ba′anib gneiss. Solid lines indicate main mineral growth during the metamorphic event. Dashed lines indicate either that the minerals are interpreted to have formed initially during M1, but recrystallized during M2 (*amphibolite), or that the mineral continued to grow during the subsequent M3 event (e.g. quartzitic schist).

contain folded ilmenite trails and are aligned parallel to S2 and S3. When fractured, they are infilled with chlorite during the D4 event. Most other minerals formed either during the peak M2 conditions or during the retrograde phase of the M2 event.

During D3 deformation, a mylonitic foliation is outlined by sericite in quartzitic schists of units II and III. The intensity of the deformation during D4 increases towards the contact of the basement to the cover nappes. Close to the contact, metapelitic schists are characterized by a matrix of chlorite which is in equilibrium with garnet, but not with staurolite and biotite, which exhibit irregular grain boundaries against chlorite. Because of the close spatial relationship of these metamorphic mineral assemblages and the structures related to the low-angle normal faulting (D4), they are interpreted to be related to an individual metamorphic event, termed M3, rather than to a retrograde phase of the M2 event. None of the mineral assemblages in the cover nappes show any indication of a high-grade metamorphic overprint (i.e. M2), but equilibrated under greenschist- to lower amphibolite facies metamorphic conditions. Therefore, the mineral assemblages in the cover nappes are considered to be part of the M3 metamorphic event.

GEOTHERMOBAROMETRY

Extensive overprinting of the M1 and M2 peak assemblages by the retrogressive M2 evolution and the M3 metamorphic event restricts the identification of equilibrated assemblages representing peak metamorphic conditions for quantitative *P–T* estimates. Therefore, calculations of the peak *P–T* conditions are restricted to the migmatized amphibolite lenses in the Um Ba′anib gneiss for M1 and some pelitic layers within units II and III of the metasedimentary sequence for M2. Peak M2 conditions are typically recorded in mineral inclusions in garnet, whereas the matrix in these schists represents the retrograde M2 phase. The M3 metamorphic event has been defined as the late-stage metamorphic equilibration associated with D4 deformation. Hence, M3 mineral assemblages occur close to the basement/cover nappe boundary, where deformation was most intense.

The mineral assemblages within the amphibolite migmatites in the Um Ba′anib gneiss equilibrated during the M2 event. Ilmenite lamellae in magnetite, which may still indicate M1 metamorphic conditions, are too fine-grained for analysis. However, melting experiments of basalts demonstrate that significant melting occurs between 750 and 800 °C at 5 kbar and H_2O-saturated conditions in these rocks (Helz, 1976). Recent fluid-absent melting experiments on island arc tholeiites indicate melting temperatures of 800 °C at 8 kbar and experiments on alkalic basalt amphibolite temperatures of 925 °C at 8 kbar, respectively (Rushmer, 1991). Therefore, a temperature estimate of at least 750–850 °C is realistic for the migmatization, because lower H_2O activities shift initial melting to higher temperatures as shown by Rushmer (1991). Hornblende/plagioclase pairs from the amphibolite xenoliths show a retrograde equilibration between 530 and 580 °C (Fig. 9) using the hornblende–plagioclase thermometer of Plyusnina (1982).

Temperatures for the M2 peak conditions were calculated using biotite inclusions in elongated garnets and in the core of a porphyroblastic garnet in sample ED50 and range from 610 to 690 °C at a reference pressure of 6 kbar (Table 6). The calibration of Hodges & Spear (1982) was used, because it corrects for the non-ideality related to Ca in garnet. The Mn content in the garnet is low (Tables 4 & 5). Virtually identical temperatures are determined, if biotite inclusions at different locations within the elongated garnets are used for calculations. Temperatures calculated using biotite inclusions from the rim of the porphyroblastic garnet in ED50 are lower than those from the core of the garnet and reflect retrograde M2 conditions. Retrograde temperatures ranging from 540 to 600 °C (Table 6) are determined using garnet rim compositions and matrix biotites.

Staurolite inclusions at the contact between the core and the rim and within the rim of a garnet in sample M138/1 and in other garnets also yield retrograde M2

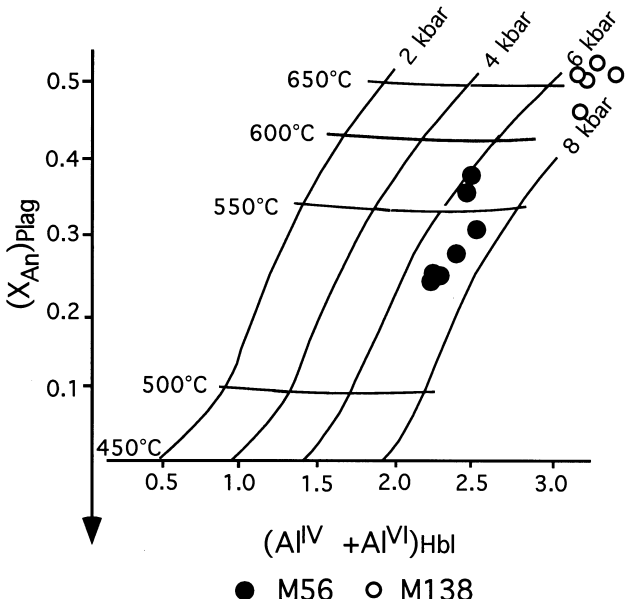

Fig. 9. Plot of amphibole–plagioclase pairs from amphibolite migmatites (sample M56) from unit I and from hornblende-plagioclase layers in sample M138/1 from unit III of the Meatiq metasedimentary rocks with respect to $(X_{An})_{Plag}$ and $(Al^{IV} + Al^{VI})_{Hbl}$ indicating M2 metamorphic temperatures and pressures (plot after Plyusnina, 1982). Plagioclase in the amphibolite migmatites is zoned. Therefore, maximum temperature estimates are the most realistic. However, temperatures derived from all plagioclase-hornblende pairs of these samples show a retrograde equilibration.

temperatures of 530–585 °C (Table 6) using the calibration of Perchuk (1991). These temperatures are consistent with the temperatures calculated using the biotite–garnet thermometer on garnet rims and matrix biotite.

Further estimates of the peak M2 temperature conditions can be made from coexisting plagioclase and hornblende in the matrix of sample M138/1 ('Hbl layer' Table 2, Fig. 9). Using the calibration of the plagioclase–hornblende thermometer of Plyusnina (1982) temperatures of 630–660 °C are estimated.

Additional constraints for the peak M2 conditions are derived from mineral reactions (Fig. 10). The mineral assemblage Kfs–Ms–Sil–Qtz indicates that the alkali feldspar forming reaction:

$$Ms + Qtz = Kfs + Al_2SiO_5 + H_2O \quad (1)$$

was reached at peak metamorphic conditions. The assemblage Ms–Kfs–Sil–Qtz indicates temperatures between 650 and 680 °C at pressures of 6–7 kbar (activity of $H_2O = 0.7$, as derived from fluid inclusions).

The mineral assemblage garnet and sillimanite in the garnet cores is replaced by staurolite at garnet rims indicating a retrograde reactions of:

$$Alm + Sil + H_2O = Fe\text{–}St + Qtz \quad (2)$$

which constrains peak temperatures to >650 °C, if pressures of >5 kbar are assumed (Fig. 10). A similar divariant reaction involving biotite, sillimanite garnet and staurolite was modelled using the computer program VERTEX (Connolly & Kerrick, 1984; Connolly, 1987; Connolly, 1990). In this reaction, grossular poor garnet coexists with sillimanite and more grossular-rich garnet with staurolite, respectively. This is consistent with the increase in the grossular component and the Fe/(Fe + Mg) ratio towards the rim (Fig. 7b) due to the temperature decrease as predicted by the modelling.

Metamorphic pressures for the M2 event have been calculated using plagioclase, muscovite and ilmenite inclusions in peak metamorphic garnets (e.g. GASP, GRIPS, GRAIL). Pressures range from 6 to 7.9 kbar for a reference temperature of 700 °C (Table 7). The pressure of 8.5 kbar, derived using the GRAIL barometer (Bohlen *et al.*, 1983) represents a maximum, because rutile is not stable in these samples (Fig. 10). Retrograde M2 pressures have been determined using garnet rims, and plagioclase and hornblende from the matrix of sample M138/1 with the Grt–Pl–Hbl–Qtz barometer of Kohn & Spear (1990). The pressures cluster around 5.8 kbar (Table 7) and vary slightly depending on the amphibole endmember chosen for recalculation.

Table 6. Summary of thermometric results from the Meatiq basement rocks.

Sample	Analyses*	Metamorphic event	Number of calculations	P (kbar) ref.	T (°C)	Mean (°C)	Setting	Remarks
Garnet-biotite thermometry (Hodges & Spear, 1982)								
ED50B	Grt20, Bt2	Peak M2	5	6	607–691	655	Grt-cores, Bt inclusions in Grt	T represents minimum for peak metamorphic temperature depending on analysis position in Grt
ED50B	Grt50/6, Bt50/6	Retrograde M2	9	5	541–604	573	Grt-rim, Bt in matrix	
M138/1		Retrograde M2	7	5	545–571	556	Grt-rim, Bt in matrix	
ED50/B	Grt24A, Bt8	M3?	1	3	482	482	Grt-rim, Bt in matrix	Estimates represent low T equilibration possibly during M3 metamorphic event
M10	Grt335, Bt43	M3	2	3	312–323	317	Grt-rim, Bt in matrix	
Garnet-staurolite thermometry (Perchuk, 1991)								
M138/1	Grt220, St42	Retrograde M2	8		532–585	552	St inclusions in Grt-rims	Estimates represent retrograde equilibration during M2 metamorphism
ED63	Grt4, St14	Retrograde M2	1		512	512	St inclusions in Grt-rims	

* Analyses listed in Tables 2, 3, 4. Further analyses used for calculation are listed in Tables A1, A2, A3.

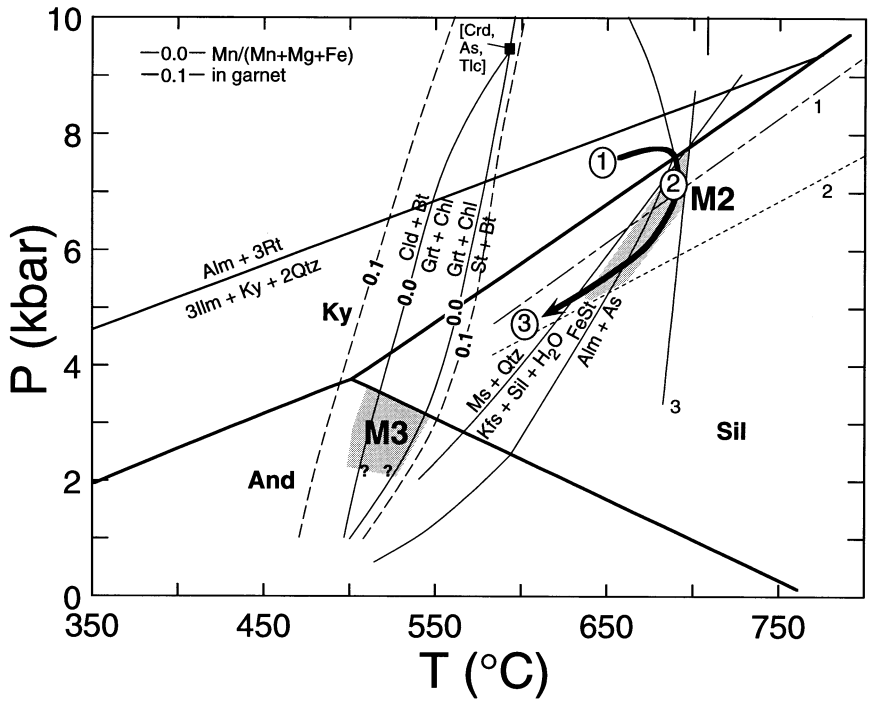

Fig. 10. Selected mineral reactions in the KFMASH petrogenetic grid (modified after Spear & Cheney, 1989 and the dataset of Berman, 1988) which are documented in the metasedimentary rocks of the Meatiq basement. The contour lines for Mn/(Mn + Mg + Fe) in garnet represent the maximum variation of the reaction, because Mn/(Mn + Mg + Fe) between 0.0 and 0.1 have been analysed in garnet. The Ms-out reaction is calculated for $a_{H2O} = 0.7$ as determined from fluid inclusions which are interpreted to represent peak metamorphic fluids. Reactions 1–3 are geothermometers and geobarometers for the metasedimentary rocks (1: Grt–Pl–Ms barometer after Hodges & Crowley, 1985; 2: Grt–Pl–Sil–Qtz after Newton & Haselton, 1981; 3: Grt–Bt thermometer for garnet cores & biotite inclusions in garnet after Hodges & Spear, 1982). Sil–Ky–And triple point after Holdaway (1971). Circled numbers refer to stages of M2 discussed in the text.

Table 7. Summary of the barometric results from the Meatiq basement rocks.

Sample	Metamorphic Analyses*	event	N	Barometer	Pressure (bar)	Setting	Reference
ED63	Grt 38, Pl 3	Peak M2	1	GASP	6485[1]	Pl, Sil inclusions in Grt cores	Newton & Haselton, 1981
ED63	Grt 38, Pl 3, Ilm 5	Peak M2	1	GRIPS	6017[1]	Pl, Sil, Ilm inclusions in Grt cores	Bohlen & Liotta, 1986
ED63	Grt 38, Ilm 5	Peak M2	1	GRAIL	8520[2]	Pl, Sil inclusions in Grt cores	Bohlen *et al.*, 1983
ED63	Grt 38, Pl 3, Ms 12	Peak M2	1	Grt-Ms-Pl-Qtz	7235[1]	Pl, Ms inclusions in Grt cores	Hodges & Crowley, 1985
ED50	Grt 24A, Pl 4, Ms 14	Peak M2	1	Grt-Ms-Pl-Qtz	7903[1]	Pl, Ms inclusions in Grt cores	Hoisch, 1990
M138/1	Grt 421, Hbl 1381, Pl 1384	Retrograde M2	1	Grt-Pl-Hbl-Qtz	5829[3] Fe endm. 5971[3] Mg endm.	Grt rims, Hbl and Pl in matrix	Kohn & Spear 1990

[1] 700 °C reference T; [2] 700 °C reference T, maximum P; [3] 600 °C T reference.

The intensity of recrystallization during the M3 metamorphic event increases towards the contact of the Meatiq basement and the ophiolite and island arc volcanic nappes in the south. Therefore, the P–T conditions attained during the M3 event can be best calculated along this contact. Postkinematic chlorite and garnet overprinted the original biotite and staurolite assemblage due to the reaction

$$St + Bt + H_2O = Grt + Chl + Ms \quad (3)$$

and is the typical M3 assemblage. This reaction was modelled by Spear & Cheney (1989) for variable X_{Mn} in garnet. Because X_{Mn} in the particular M3 garnet rims is <0.1, temperatures of below 550 °C (assuming $P<4$ kbar) can be estimated (Fig. 10).

P–T conditions during M3 in the ophiolite nappes are difficult to constrain due to the lack of P–T sensitive mineral assemblages. However, maximum metamorphic temperatures in the serpentinites are constrained by the upper stability of antigorite according to the reaction

$$Atg = Fo + Tlc + H_2O \quad (4)$$

to <540 °C assuming maximum pressures of 4 kbar (Johannes, 1969). Because chrysotile has not formed in these samples, minimum temperatures are constrained to about 300–350 °C by the same assemblage. Metamorphic actinolite in rims around magmatic hornblende in the Abu Fannani metatonalites from Panafrican nappes on top of the Meatiq basement south of G. Meatiq (Fig. 1) are consistent with a greenschist facies M3 event.

METAMORPHIC FLUIDS

Fluid inclusion data have been collected using a computer-controlled Linkham THMSG 600 heating/freezing stage at the Institute of Mineralogy-Crystallography and Petrology at the Karl-Franzens University Graz. The heating/freezing stage was calibrated initially using commercially available calibration standards Toluol (−95 °C), pure CO_2 (−56.6 °C), *n*-Decan (−29.7 °C), *n*-Dodecan (−9.6 °C), pure H_2O (0.0 °C), Merck 9640 (+40.0 °C), Merck 9665 (+65.0 °C), Merck 9685 (+85.0 °C), Merck 9730 (+130.0 °C), Merck 9780 (+180.0 °C), Merck 9800 (+200.0 °C) and Sodium nitrate (+306.8 °C) to ensure accuracy and precision of the data. The calibration of the heating/freezing stage was then checked prior to each analytical session using the CO_2-freezing point at −56.6 °C. Reproducibility is 0.2 °C at a heating rate of 0.1 °C/min. All measurements were corrected using the determined calibration curves (MacDonald & Spooner, 1981).

Fluid inclusions in quartz included in peak M2 garnet and in the vicinity of the garnet have been investigated to gain information on the composition of the M2 metamorphic fluids and the *P–T* paths during M2 metamorphism. Quartz inclusions in M2 garnet are more likely to have trapped and preserved peak metamorphic fluids, because the rock matrix has been affected by later deformation events. Therefore, fluid inclusions in the matrix consist of peak and retrograde fluids. Samples have been selected from zones I (Um Ba′anib gneiss), II (spinel bearing quartzitic Grt–Ms schist) and III (Bt–Grt schist; cf. Fig 2).

Four types of fluid inclusions are distinguished in all three zones using petrographic observations and microthermometric data:
Type 1: water dominated aqueous-carbonic fluids (H_2O-$CO_2 \pm CH_4$ and/or N_2);
Type 2: CO_2 dominated aqueous-carbonic fluids (CO_2-$H_2O \pm CH_4$ and/or N_2);
Type 3: carbonic fluids (CO_2-CH_4 and/or N_2);
Type 4: aqueous fluids (H_2O).

Type 1 occurs mainly as single inclusions or clusters particularly in the quartz inclusions in garnet, whereas Type 2 and 3 occur dominantly in trails and subordinately in clusters in the matrix. Type 4 inclusions occur almost exclusively in trails which typically cross quartz grain boundaries in the matrix and are therefore considered to be late.

Microthermometric data of fluid inclusions of samples from all three zones are summarized in Fig. 11. Type 1–3 inclusions differ mainly in their CO_2 content from dominantly H_2O with minor CO_2 in Type 1 inclusions to dominantly carbonic ($CO_2 \pm CH_4 \pm N_2$) in Type 3 inclusions. Melting temperatures of CO_2 ice range in all three fluid inclusion types from −56.6 to −57.7 °C which indicates only a minor component of another gaseous phase, probably CH_4 and/or N_2. The clathrate of CO_2 melts between 7 and 10 °C which corresponds to a salt content of 0–6 wt% NaCl equivalent (Diamond, 1992). Homogenization of CO_2 occurs between 22 and 30 °C mostly to the liquid phase and total homogenization occurs between 280 and 305 °C to the liquid phase. This results in bulk densities from 0.5–0.85 g/cm^3 for Type 2 and 3 inclusions and 0.75–0.95 g/cm^3 for Type 1 inclusions. The melting of H_2O ice in Type 4 aqueous inclusions occurs between −6 and 0 °C which corresponds to a NaCl content of 0–10 wt% NaCl equivalent (Brown, 1989; and references therein). Total homogenization temperatures range from 140 to 250 °C.

The variation in the CO_2/H_2O ratio in the Type 1–3 inclusions may be related to: (1) retrograde modification of an originally H_2O dominant H_2O-CO_2 fluid, (2) high-temperature phase separation of a combined H_2O-CO_2 fluid, or (3) real variations in the fluid composition as the metamorphic core complex evolves from high to low-metamorphic conditions. Retrograde modifications can be related to preferential H_2O loss either due to microfracturing during deformation, diffusional processes, or wetting out of H_2O due to grain boundary migration and recrystallization (Bodnar *et al*., 1989; Hollister, 1990; Hall *et al*., 1991; Johnson & Hollister, 1995; Klemd *et al*., 1995).

Deformational microfracturing and subsequent H_2O loss results in a size reduction of the fluid inclusions (Hollister, 1990). However, the size of Type 1–3 inclusions and the CO_2/H_2O ratio do not correlate (Fig. 12), indicating that this process is less likely to have occurred. Preferential H_2O loss due to retrograde equilibration and diffusional processes should increase the salinity of the remaining H_2O in the fluid inclusion (Hall & Sterner, 1993). This process is also unlikely to have occurred within Type 1–3 inclusions, because salinity and fluid inclusions size show only a poor correlation trend, if any (Fig. 12). Water loss from the fluid inclusions due to quartz recrystallization cannot be excluded and may be indicated by positive correlation of Th_{CO2} and the inclusions size (Fig. 12). This correlation is due to the fact that larger inclusions re-equilibrate before smaller ones (Bodnar *et al*., 1989; Hall *et al*., 1991). However, in this case the *P–T* information in the fluid inclusions would indicate the conditions of recrystallization and fluid inclusions should monitor the retrograde cooling path (Johnson & Hollister, 1995). High-temperature phase separation of a mixed CO_2-H_2O fluid is less likely to have occurred, because observed salinities in the H_2O-rich endmembers are low and do not show any correlational trend with the CO_2/H_2O ratio (Fig. 12).

Of the isochores calculated for Type 1–3 inclusions using the computer program FLINCOR (Brown, 1989) the Type 1 (H_2O-rich, CO_2-poor) isochores are steepest. Type 2 and 3 inclusions are characterized by slopes which tend to be flatter with higher CO_2 content of the fluid inclusions. Isochores for the Type 4 aqueous inclusions show a steeper slope then Type 1 inclusions.

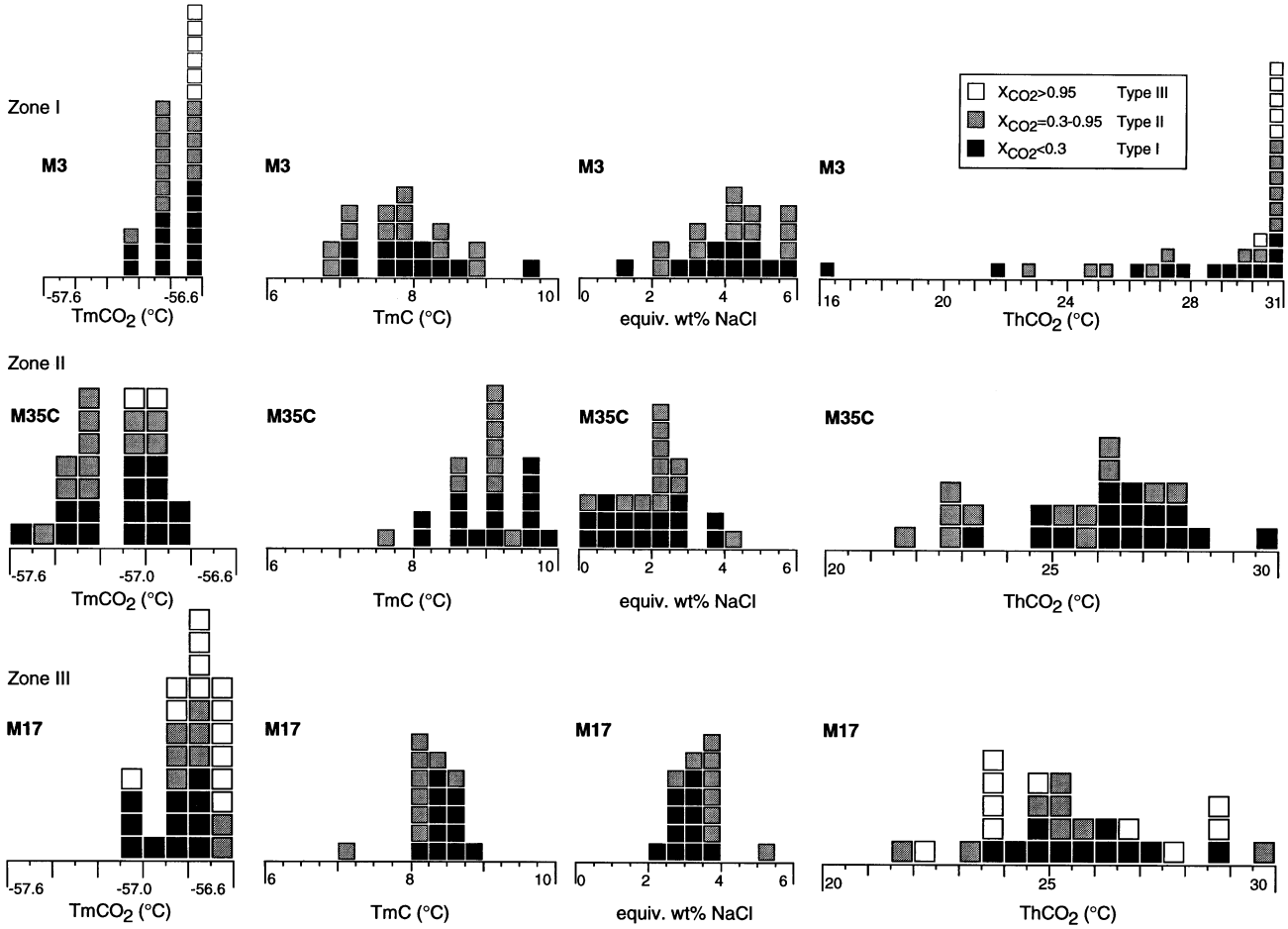

Fig. 11. Histograms for $TmCO_2$, TmC (clathrate), equiv. wt% NaCl and $ThCO_2$ for Type 1–3 fluid inclusions in quartz in the Um Ba'anib gneiss (unit I, sample M3), and the units II (sample M35C) and III (sample M17) from the Meatiq metasedimentary rocks.

Type 1 inclusions with the highest density are interpreted to represent peak M2 metamorphic or marginally retrograde fluids, because the isochores of these inclusions pass through the lower part of the peak M2 *P–T* conditions. In addition, these inclusions occur dominantly as single inclusions or in clusters. Types 2 and 3 inclusions plus those Type 1 inclusions which are characterized by isochores below the peak *P–T* field, are interpreted to represent fluids which have either been trapped during retrograde M2 or earlier, but were modified during the retrogade conditions. Type 4 inclusions occur in trails which typically cut across quartz grain boundaries, and are interpreted to represent either the latest M2 or, more likely, M3 metamorphic fluids and may be similar to fluids trapped below the brittle/ductile transition (cf. Johnson & Hollister, 1995).

DISCUSSION AND INTERPRETATION

P–T–t paths

Due to poor constraints on the *P–T* evolution of M1, metamorphic *P–T–t* paths can only be estimated for the M2 and M3 metamorphic events. Kyanite, which is locally preserved as relics, was stable during peak pressures of the M2 event (stage 1, Fig. 10). However, most peak M2 temperature assemblages contain sillimanite (stage 2, Fig. 10). Reaction textures of fibrolitic sillimanite overgrowth of relictic kyanite and clusters of sillimanite representing pseudomorphs after kyanite are indicative of this sequence. Andalusite formed after sillimanite in retrograde M2 assemblages, documented in andalusite pseudomorphs after sillimanite needles (stage 3, Fig. 10). In addition, andalusite typically rims sillimanite clusters. Retrograde pressure conditions are constrained by andalusite to <4 kbar (Holdaway, 1971; Bohlen *et al.*, 1991), whereas peak M2 pressures are estimated as 6–8.5 kbar. Together, all evidence from mineral assemblages indicate a clockwise *P–T* path for the M2 metamorphic event.

M2 fluid inclusion show an array from steep isochores, which can be correlated with peak or slightly retrograde M2 conditions, to flat isochores representing fluid inclusions trapped during retrograde M2 conditions (Fig. 13). This array is interpreted to represent a *clockwise P–T* evolution during the M2 metamorphic

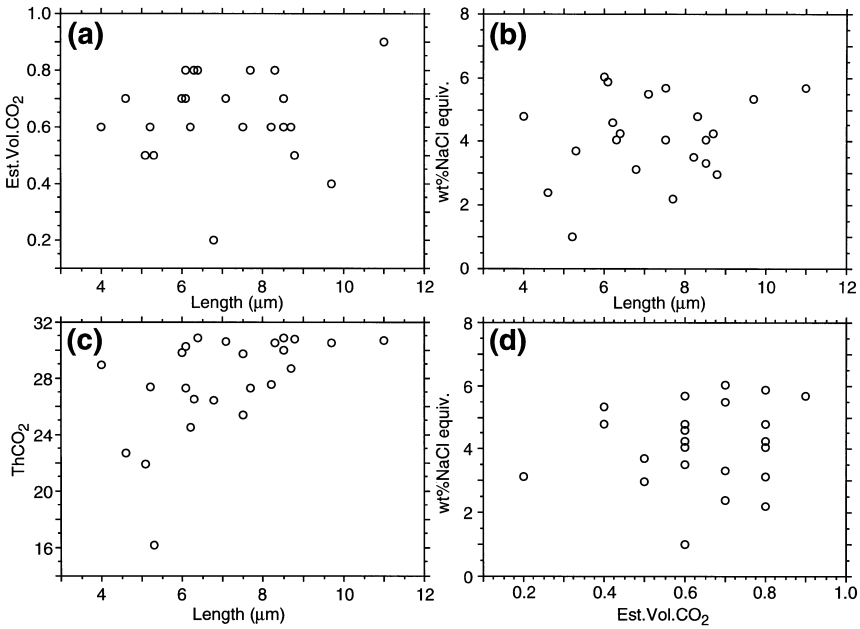

Fig. 12. Scattergrams of estimated volume fractions (a) CO_2 (b) salinity, and (c) $ThCO_2$ vs. fluid inclusion size and (d) salinity vs. volume fractions CO_2 for sample M3. This is representative for all other samples investigated for fluid inclusions which show similar trends.

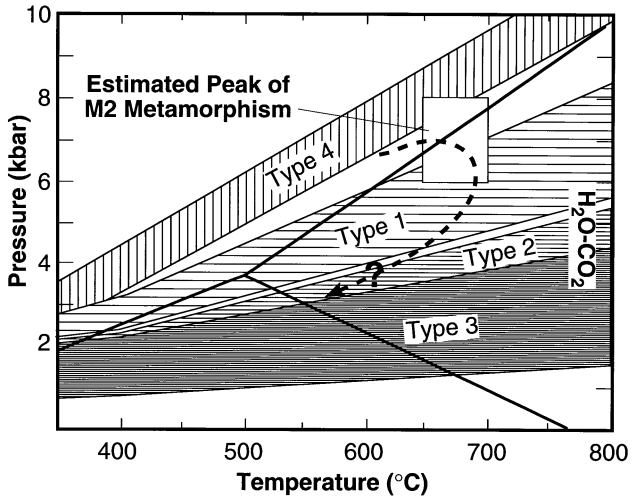

Fig. 13. Isochores for Type 1–3 (H_2O-$CO_2 \pm CH_4 \pm N_2$) and Type 4 (H_2O) inclusions from samples of the Um Ba′anib gneiss and the units II and III of the Meatiq metasedimentary rocks. Type 1–3 inclusions are hosted in quartz inclusions in peak M2 metamorphic garnet or occur adjacent to these garnets, whereas Type 4 inclusions are hosted in the matrix quartz only. Thick solid lines represent the Sil–Ky–And triple point after Holdaway (1971).

event. Therefore, constraints on the *P–T–t* path derived from fluid inclusions are consistent with those derived from mineral assemblages.

The prograde evolution of the M2 event is documented by the formation of a first generation of staurolite for which the evidence is interpenetration twin-like habits of elongated garnet crystals, hosting inclusions of Zn-rich spinel in unit II (stage 1, Fig. 10). This texture and the mineral assemblage Grt–Sil–Zn–Spl (sample NM116, Table 2) indicate that both garnet and spinel formed from staurolite at, or close to, the temperature peak according to the reaction (Fig. 10):

$$(Zn)\text{–}St = Alm + Sil + (Zn)\text{–}Spl + H_2O \qquad (5)$$

or in similar reactions forming either garnet or spinel (e.g. Ganguly, 1972).

The peak temperature stage of M2 (stage 2, Fig. 10) is preserved in the chemical composition of garnet (Fig. 6). Homogeneous chemical profiles across garnet cores (Fig. 6) indicate either garnet growth during fixed *P–T* conditions by univariant reactions or, more likely, diffusional equilibration at high temperatures destroying growth zoning (e.g. Chakraborty & Ganguly, 1991; and references therein). Yardley (1977) estimates temperatures for beginning diffusional processes to be >640 °C, but claims that $T>700$ °C are necessary for efficient diffusional equilibration. Mn-rich cores of some garnet (Fig. 7) are interpreted to indicate either preservation of prograde zonation during peak metamorphic conditions or Mn enrichment due to Raleigh fractionation (e.g. Harte & Henley, 1966; Hollister, 1966). Only minor variations in the chemical profile in zone A2 (Fig. 7) indicate that this zone equilibrated chemically at high temperature due to diffusion. However, diffusional equilibration did not progress to the core of the garnet, because of its large size and hence prograde chemical zonation is still preserved in the core.

The retrograde stage of the M2 event (stage 3, Fig. 10) is documented by the increase of Ca and Mn towards the garnet rim (Fig. 6) which probably results

from the formation of relatively Mn and Ca poor minerals such as biotite and a second generation of staurolite (Tracy, 1982; Loomis, 1983 and references therein). Inclusions of staurolite occur within the rims of the garnet (Figs 5d & 6), but are absent in the core indicating the formation of retrograde staurolite according to reaction 4. In addition, the increase in Fe/(Fe + Mg) in garnet from core to rim may be related to the formation of staurolite ($X_{Fe} = 0.81$). The formation of retrograde staurolite is also documented by the abundant staurolite in the rock matrix.

In summary, the clockwise M2 evolution must be split into three stages; a first high-P/T stage with staurolite and kyanite (present as pseudomorphs or relics, respectively), a second stage of increasing temperature overstepping the staurolite-out reaction and characterized by spinel, sillimanite, ± alkali feldspar and garnet formation, and a third stage of retrogressive staurolite formation which leads to the documented mineral assemblage of the matrix.

Tectonic implications

In this study, distinct differences in the metamorphic evolution of the Meatiq basement and the covering ophiolite and island arc volcanic nappes have been determined. Three metamorphic events, an anatectic event, an upper amphibolite facies event and a low-grade, upper-greenschist facies event, occurred in the basement. In contrast, the covering nappes have been metamorphosed only once, during the latest greenschist facies metamorphic event. All evidence suggests that a distinct metamorphic break in the metamorphic evolution exists between the basement and the covering nappes. Therefore, the Meatiq basement complex is also in its metamorphic setting similar to metamorphic core complexes in the Cordilleran.

There are a number of lines of evidence which indicate that the formation of the precursor rocks of the amphibolite xenoliths within the Um Ba′anib gneiss occurred probably in an extensional tectonic environment. The chemical composition of these amphibolites permits the distinction of two tectonic groups (Neumayr *et al.*, 1996). One group formed in a within-plate tectonic environment, whereas the other group shows typical N-type MORB characteristics. The complexity of the chemical composition of these amphibolites indicates the formation of oceanic crust and within-plate magmatism prior to the intrusion of the Um Ba′anib granitoid (Neumayr *et al.*, 1996). The age of the Um Ba′anib granitoid is constrained by a probable magmatic age of ≈780 Ma (U. Klötzli, personal com., 1996; Pb single zircon evaporation). Therefore, the amphibolite xenoliths are older than 780 Ma. Stern (1994) concluded in a compilation of 10 isotopic ages for ophiolites from Egypt and Sudan that ophiolites formed from 880 to 690 Ma with two maxima from 850 to 800 Ma and from 750 to 700 Ma. Therefore, the amphibolite xenoliths formed probably during the first period of ophiolite formation reported by Stern (1994). However, little evidence is preserved for the tectonic setting in which the M1 migmatization event occurred.

The formation of the oceanic crust, which finally forms part of the ophiolitic mélange on top of the basement, may have occurred during the second period reported by Stern (1994). The collision and incipient thrusting is constrained to have occurred between the age of the Um Ba′anib granitoid (780 Ma) and the oldest syntectonic granite in the Meatiq basement (626 Ma, Table 1). Prograde M2 evolution probably occurred during the collision of the island arc (documented in the acid volcanic rocks to the east of the Meatiq basement; El Ramly, 1972) and the basement domain and caused a P–T path along a normal geotherm into the kyanite field (Pollack & Chapman, 1977; Fig. 14a & b) where the first equilibrium assemblage of M2 crystallized (stage 1, Fig. 10). The subsequent heat input (stage 2, Fig. 10) which changed the assemblage to high temperature phases could have been triggered by break-off of the subducting slab (e.g. Davies & von Blanckenburg, 1995), which caused the rise of the asthenosphere and the increase in temperature in the Meatiq basement (Fig. 14b & c). This would result in heating without further pressure increase leading to transformation of kyanite into sillimanite and overstepping of the staurolite-out and muscovite-alkali feldspar-out reactions (e.g. Warren & Ellis, 1996). Meanwhile thrusting in the obducted ophiolite mélange continued towards the foreland (Fritz *et al.*, 1996; Messner *et al.*, 1996).

Magmatic underplating, caused by the rise of the asthenosphere and the associated temperature increase, initiated the rise of granitoid intrusions and, consequently, also the Meatiq basement (e.g. Warren & Ellis, 1996; Fig. 14d). Abundant granitoid magmatism is documented throughout the Eastern Desert of Egypt, for example in the Hafafit basment around 700 Ma (Kröner *et al.*, 1994), the Sibai culmination between 660 and 630 Ma (U. Klötzli, personal com., 1996) and the Meatiq basement between 644 Ma (syntectonic granitoids) and 580 Ma (post-tectonic granitoids; U. Klötzli, personal com., 1997; Table 1). D3 planar fabrics and L3 stretching lineations formed during this uplift of the basement during the retrograde phase of the M2 metamorphic event (Fig. 14e) leading to an adjustment of the mineral assemblages to decreasing temperatures and pressures (stage 3, Fig. 10).

The initiation of the strike-slip faulting and N- and S- directed low-angle normal faults resulted in the final uplift of the Meatiq basement (Fritz *et al.*, 1996) and the M3 greenschist facies metamorphic event which is most pronounced close to, and along, the D4 normal faults (Fig. 14e & f). The age of the early normal faults is constrained by the syntectonic granitoids at the southern margin of the Meatiq basement to 614 Ma (Stern & Hedge, 1985), and final cooling is constrained to about 590 Ma (Fritz *et al.*, 1996)

The metamorphic evolution of the Meatiq basement

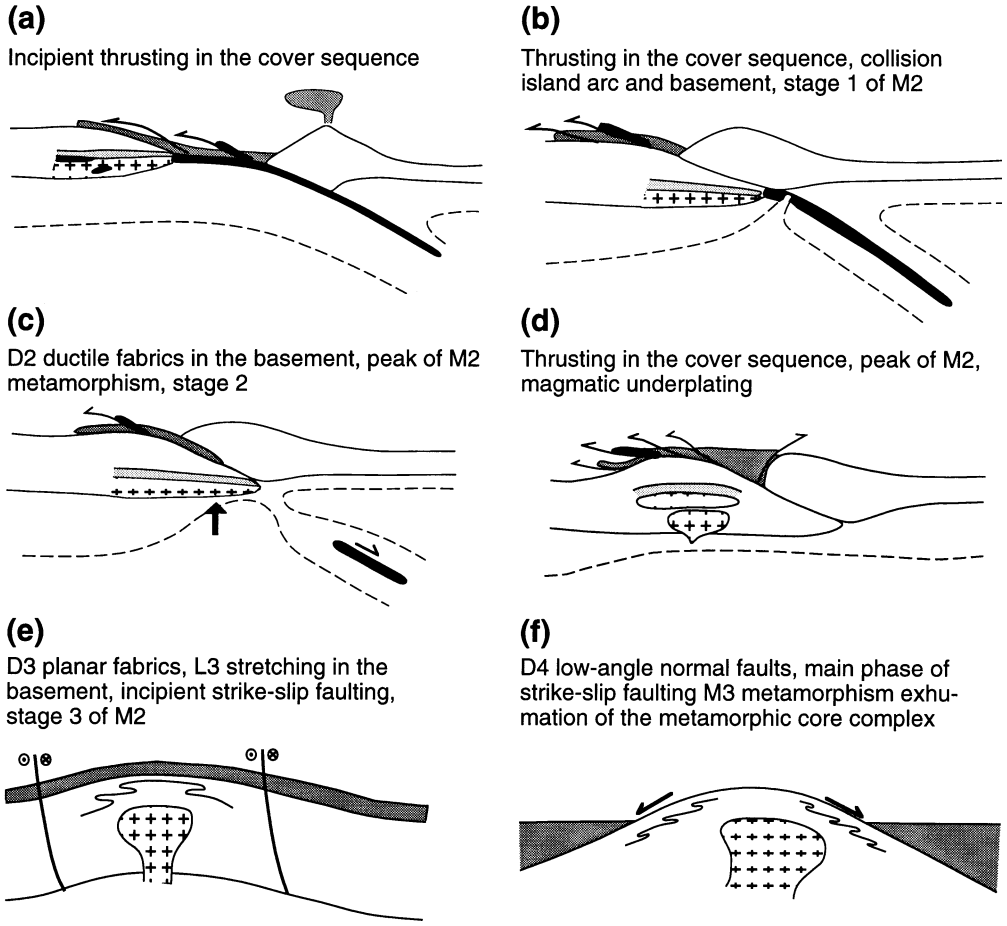

Fig. 14. Sketches of the interpreted tectonic evolution of the Meatiq metamorphic core complex. (a) Incipient thrusting of the ophiolite mélange on to the basement, subsequent to M1 metamorphism and the intrusion of the Um Ba′anib granitoid at *c.* 780 Ma; (b) Collision of the island arc and the basement, thrusting in the cover nappes; prograde evolution of the Meatiq basement (Um Ba′anib granitoid, amphibolite xenoliths, sedimentary cover) and possible slab break-off of the subducting oceanic crust; (c) development of the D2 ductile fabrics and peak temperature of the M2 metamorphic event due to the rise of the asthenosphere and the temperature increase; thrusting in the cover nappes; (d) magmatic underplating causes the rise of granitoid intrusions and uplift of the Meatiq dome; (e) development of D3 planar and S3 linear fabrics in the basement due to the rise of the basement; Incipient strike-slip faulting; retrograde M2 conditions; (f) N- and S-directed low-angle normal faults at the top of the basement and M3 metamorphism which is particularly pronounced in the upper section of the basement. Profiles A-E are orientated W-E and profile F N-S, respectively.

dome can be correlated with a complex structural history of the area. It is important to note that the metamorphic history is inconsistent with the formation of the basement and the cover nappes in a single orogenic cycle, although precise isotopic constraints on the different metamorphic events are largely missing. A more detailed interpretation, involving an early extension to form the precursor of the amphibolite xenoliths, a collisional event during which M2 took place and a final extensional event causing uplift and exhumation of the metamorphic core complex, is consistent with the metamorphic evolution determined in this study.

ACKNOWLEDGEMENTS

This study is part of the FWF-project P09703-GEO and is financed by the Austrian 'Fonds zur Förderung der wissenschaftlichen Forschung'. Discussions and help from all other project members of the Department of Geology and Palaeontology, Karl-Franzens University Graz are gratefully acknowledged. The authors also acknowlegde the logistic support by the University of Assiut (Egypt), particularly by Prof. Dr S. El Gaby. Critical comments on an earlier version of this paper by R. Klemd, A. Möller and J. R. Ridley are greatfully acknowledged.

REFERENCES

Berman, R. G., 1988. Internally consistent thermodynamic data for minerals in the system SiO_2-K_2O-Na_2O-Fe_2O_3-TiO_2-Al_2O_3-FeO-MgO-K_2O-H_2O-CO_2. *Journal of Petrology*, **29,** 445–522.

Bodnar, R. J., Binns, P. R. & Hall, D. L., 1989. Synthetic fluid inclusions, VI. Quantitative evaluation of the description behaviour of fluid inclusions in quartz at one atmosphere

confining pressure. *Journal of Metamorphic Geology*, **7,** 229–242.
Bohlen, S. R. & Liotta, J. J., 1986. A barometer for garnet amphibolites and garnet granulites. *Journal of Petrology*, **27,** 1025–1034.
Bohlen, S. R., Wall, V. T. & Boettcher, A. L., 1983. Experimental investigations and geological applications of equilibria in the system FeO-TiO_2-Al_2O_3-SiO_2-H_2O. *American Mineralogist*, **68,** 1049–1058.
Bohlen, S. R., Montana, A. & Kerrick, D. M., 1991. Precise determinations of the equilibrium kyanite = andalusite and a revised tripple point for Al_2SiO_5 polymorphs. *American Mineralogist*, **76,** 677–680.
Brown, P. E., 1989. FLINCOR: A microcomputer program for the reduction and investigation of fluid inclusion data. *American Mineralogist*, **74,** 1390–1393.
Chakraborty, S. & Ganguly, J., 1991. Compositional zoning and cation diffusion in garnets. In: *Diffusion, Atomic Ordering and Mass Transport – Selected Topics in Geochemistry* (ed. Ganguly, J.), pp. 120–175. Springer Verlag, Berlin, Heidelberg, New York.
Coney, P. J., 1980. Cordilleran metamorphic core complexes: An overview. *Geological Society of America Memoir*, **153,** 7-31.
Connolly, J. A. D., 1987. An algorithm and computer program for calculating composition phase diagrams. *CALPHAD*, **11,** 1-61.
Connolly, J. A. D., 1990. Multivariable phasediagrams; an algorithm based on generalized thermodynamics. *American Journal of Science*, **290,** 666–718.
Connolly, J. A. D. & Kerrick, D. M., 1984. VERTEX: A computer algorithm for the calculation of stable phase assemblages and Schreinemakers-type phase diagrams. *EOS*, **65,** 287.
Crittenden, M. D., Coney, P. J. & Davies, G. H., 1980. Cordilleran metamorphic core complexes. *Geological Society of America Memoir*, **153,** 490.
Davies, J. H. & von Blanckenburg, F., 1995. Slab breakoff: A model of lithosphere detachment and its test in the magmatism and deformation of collisional orogens. *Earth and Planetary Science Letters*, **129,** 85–102.
Diamond, L. D., 1992. Stability of CO_2 clathrate hydrate + CO_2 liquid + CO_2 vapour + aqueous KCl-NaCl solutions: Experimental determination and application to salinity estimates of fluid inclusions. *Geochimica Cosmochimica Acta*, **56,** 273–380.
El Gaby, S., List, F. K. & Tehrani, R., 1990. The basement complex of the Eastern Desert and Sinai. In: *The Geology of Egypt* (ed. Rushdi, S.), pp. 175–184. Balkema, Rotterdam.
El Ramly, I. M., 1972. A new geological map for the basement rocks in the eastern and southwestern deserts of Egypt, scale, 1 : 1000000. *Annuals of the Geological Survey of Egypt*, **2,** 1–18.
Fritz, H., Wallbrecher, E., Khudeir, A. A., El Ela, F. A. & Dallmeyer, D. R., 1996. Formation of Neoproterozoic metamorphic core complexes during oblique convergence (Eastern Desert, Egypt). *Journal of African Earth Sciences*, **23,** 311–329.
Ganguly, J., 1972. Staurolite, stability and related parageneses: Theory, experiments, and applications. *Journal of Petrology*, **13,** 335–365.
Greiling, R. O., Abdeen, M. M., Dardir, A. A., El Akhal, H., El Ramly, M. F., Kamal El Din, G. M., Osman, A. F., Rashwan, A. A., Rice, A. H. N. & Sadek, M. F., 1994. A structural synthesis of the Proterozoic Arabian-Nubian Shield in Egypt. *Geologische Rundschau*, **83,** 484–501.
Habib, M. E., Ahmed, A. A. & El Nady, O. M., 1985. Two orogenies in the Meatiq Area of the Central Eastern Desert, Egypt. *Precambrian Research*, **30,** 83–111.
Hall, D. L. & Sterner, S. M., 1993. Preferential water loss from synthetic fluid inclusions. *Contributions to Mineralogy and Petrology*, **114,** 489–500.
Hall, D. L., Bodnar, R. J. & Craig, J. R., 1991. Fluid inclusion constraints on the uplift history of the metamorphosed massive sulphide deposits at Ducktown, Tennesee. *Journal of Metamorphic Geology*, **9,** 551–565.
Harte, B. & Henley, K. J., 1966. Occurrence of compositionally zoned almanditic garnets in regionally metamorphosed rocks. *Nature*, **210,** 689–692.
Helz, R. T., 1976. Phase relations of basalts in their melting ranges at $PH_2O = 5$ kb. Part 1. Melt compositions. *Journal of Petrology*, **17,** 139–193.
Hodges, K. V. & Crowley, P. D., 1985. Error estimation and empirical geothermobarometry for pelitic systems. *American Mineralogist*, **70,** 702–709.
Hodges, K. V. & Spear, F. S., 1982. Geothermometry, geobarometry and the Al_2SiO_5 tripple point at Mt. Moosilauke, New Hampshire. *American Mineralogist*, **67,** 1118–1134.
Hoisch, T. D., 1990. Empirical calibration of six geobarometers for the mineral assemblage quart + muscovite + biotite + plagioclase + garnet. *Contributions to Mineralogy and Petrology*, **104,** 225–234.
Holdaway, M. J., 1971. Stability of andalusite and the aluminum silicate phase diagram. *American Journal of Science*, **271,** 97-131.
Hollister, L. S., 1966. Garnet zoning: an interpretation based on the Raleigh fractionation model. *Science*, **154,** 1647–1651.
Hollister, L. S., 1990. Enrichment of CO_2 in fluid inclusions in quartz by removal of H_2O during crystal-plastic deformation. *Journal of Structural Geology*, **12,** 895–901.
Johannes, W., 1969. An experimental investigation of the system MgO-SiO_2-H_2O-CO_2. *American Journal of Science*, **267,** 1083–1104.
Johnson, E. L. & Hollister, L. S., 1995. Syndeformational fluid trapping in quartz: determining the pressure-temperature conditions of deformation from fluid inclusions and the formation of pure CO2 fluid inclusions during grain-boundary migration. *Journal of Metamorphic Geology*, **13,** 239–249.
Klemd, R., Bröcker, M. & Schramm, J., 1995. Characterisation of amphibolite-facies fluids of Variscan eclogites from the Orlica-Snieznik dome (Sudetes, SW Poland). *Chemical Geology*, **119,** 101–113.
Kohn, M. J. & Spear, F. S., 1990. Two new barometers for garnet amphibolites with applications to eastern Vermont. *American Mineralogist*, **75,** 89–96.
Kröner, A., Krüger, J. & Rashwan, A. A., 1994. Age and tectonic setting of granitoid gneisses in the Eastern Desert of Egypt and south-west Sinai. *Geologische Rundschau*, **83,** 502–513.
Kretz, R., 1983. Symbols for rock-forming minerals. *American Mineralogist*, **68,** 277–279.
Leake, B. E., 1978. Nomenclature of amphiboles. *Mineralogical Magazine*, **42,** 533–563.
Lister, G. S. & Davis, G. B., 1989. The origin of metamorphic core complexes and detachment faults formed during Tertiary continental extension in the northern Colorado region, U.S.A. *Journal of Structural Geology*, **11,** 65–94.
Loomis, T. P., 1983. Metamorphic petrology. *Reviews of Geophysics*, **21,** 1386–1394.
MacDonald, A. J. & Spooner, E. T. C., 1981. Calibration of a Linkam TH 600 Progammable heating-cooling stage for microthermometric examination of fluid inclusions. *Economic Geology*, **76,** 1248–1258.
Messner, M., Fritz, H., Pelz, K. & Unzog, W., 1996. Beckenbildung in verschiedenen tektonischen Settings: Struktureller Rahmen und Abbildung der Tektonik in der Sedimentation. In: *TSK, Symposium für Tektonik, Struktur- und Kristallingeologie*, pp. 275–278, Salzburg.
Morimoto, N., 1988. Nomenclature of pyroxenes. *Mineralogy and Petrology*, **39,** 55–76.
Neubauer, F., Dallmeyer, R. D., Schiernik, D. & Dunkl, I., 1994. Late Cretaceous uplift of the metamorphic Gleinalm dome Eastern Alps. Cooling history and sedimentary response in a sinistral wrench corridor. *Tectonophysics*, **242,** 79–98.
Neumayr, P., Mogessie, A., Hoinkes, G. & Puhl, J., 1996. Geological Setting of the Meatiq metamorphic core complex in the Eastern Desert of Egypt based on amphibolite geochemistry. *Journal of African Earth Sciences*, **23,** 331–345.
Newton, R. C. & Haselton, H. T., 1981. Thermodynamics of

the garnet-plagioclase-Al_2SiO_5-quartz geobarometer. In: *Thermodynamics of Minerals and Melts* (ed. Newton, R. C.), pp. 131–147. Springer Verlag, New York.

Perchuk, L. L., 1991. Mineral thermodynamics and equilibria for geothermobarometry: an introduction. In: *Progress in Metamorphic and Magmatic Petrology* (ed. Perchuk, L.L.), pp. 503. Cambridge University Press, Cambridge.

Platt, J. P., 1986. Dynamics of orogenic wedges and the uplift of high-pressure metamorphic rocks. *Geological Society of America Bulletin*, **97,** 1037–1053.

Plyusnina, L. P., 1982. Geothermometry and Geobarometry of plagioclase-hornblende bearing assemblages. *Contributions to Mineralogy and Petrology*, **80,** 140–146.

Pollack, H. N. & Chapman, D. S., 1977. On the regional variation of heat flow, geotherms and lithosphere thickness. *Tectonophysics*, **38,** 279–296.

Ries, A. C., Shackleton, R. M., Graham, R. H. & Fitches, W. R., 1983. Pan-african structures, ophiolites and mélange in the Eastern Desert of Egypt: a traverse at 26° N. *Journal of the Geological Society of London*, **140,** 75–95.

Rushmer, T., 1991. Partial melting of two amphibolites: contrasting experimental results under fluid-absent conditions. *Contributions to Mineralogy and Petrology*, **107,** 41–59.

Shackleton, R. M., Ries, A. C., Graham, R. H. & Fitches, W. R., 1980. Late Precambrian ophiolite melange in the Eastern Desert of Egypt. *Nature*, **285,** 472–474.

Spear, F. S. & Cheney, J. T., 1989. A petrogenetic grid for pelitic schists in the system SiO_2-Al_2O_3-FeO-MgO-K_2O-H_2O. *Contributions to Mineralogy and Petrology*, **101,** 149–164.

Stern, R. J., 1994. Arc Assembly and continental collision in the Neoproterozoic East African Orogen: Implications for the consolidation of Gondwanaland. *Annual Reviews Earth and Planetary Science Letters*, **22,** 319–351.

Stern, R. J. & Hedge, C. E., 1985. Geochronologic and isotopic constraints on late Precambrian crustal evolution in the Eastern Desert of Egypt. *American Journal of Science*, **285,** 97-127.

Sturchio, N. C., Sultan, M. & Batiza, R., 1983a. Geology and origin of Meatiq Dome, Egypt: A Precambrian metamorphic core complex? *Geology*, **11,** 72–76.

Sturchio, N. C., Sultan, M., Sylvester, P., Batiza, R., Hedge, C., El-Shazly, E. M. & Abdel-Meguid, A., 1983b. Geology, age, and origin of Meatiq Dome: Implications for the Precambrian stratigraphy and tectonic evolution of the Eastern Desert of Egypt. In: *Geology, Age, and Origin of Meatiq Dome: Implications for the Precambrian Stratigraphy and Tectonic Evolution of the Eastern Desert of Egypt* (ed. Al-Shanti, A. M.). King Abdulasiz University Faculty of Earth Sciences, Bulletin 6.

Tracy, R. J., 1982. Compositional zoning and inclusions in metamorphic minerals. *Reviews in Mineralogy*, **10,** 355–397.

Vissers, R. M. L., Platt, J. P. & van der Wal, D., 1995. Late orogenic extension of the Betic Cordillera and the Alboran Domain: A lithospheric view. *Tectonics*, **14,** 786–803.

Wallbrecher, E., Fritz, H., Khudeir, A. A. & Farahad, F., 1993. Kinetics of Panafrican thrusting and extension in Egypt. In: *Geoscientific Research in Northeast Africa* (eds Thorweihe, U. & Schandelmeier, H.), pp. 27–30. Balkema, Rotterdam.

Warren, R. G. & Ellis, D. J., 1996. Mantle underplating, granite tectonics and metamorphic P-T-t paths. *Geology*, **24,** 663–666.

Wijbrans, J. R., van Wees, J. D., Stephenson, R. A. & Cloetingh, S. A. P. L., 1993. Pressure-Temperature-time evolution of the high pressure metamorphic complex of Sifnos, Greece. *Geology*, **21,** 443–446.

Yardley, B. W. D., 1977. An empirical study of diffusion in garnet. *American Mineralogist*, **62,** 793–800.

Received 26 February 1996; revision accepted 20 September 1997.